

Structural insights into Ubr1-mediated N-degron polyubiquitination

<https://doi.org/10.1038/s41586-021-04097-8>

Received: 15 April 2021

Accepted: 6 October 2021

Published online: 17 November 2021

 Check for updates

Man Pan^{1,5} , Qingyun Zheng^{2,3,5}, Tian Wang^{2,5}, Lujun Liang^{2,5}, Junxiong Mao², Chong Zuo², Ruichao Ding², Huasong Ai², Yuan Xie¹, Dong Si⁴, Yuanyuan Yu^{1,3} , Lei Liu²  & Minglei Zhao¹ 

The N-degron pathway targets proteins that bear a destabilizing residue at the N terminus for proteasome-dependent degradation¹. In yeast, Ubr1—a single-subunit E3 ligase—is responsible for the Arg/N-degron pathway². How Ubr1 mediates the initiation of ubiquitination and the elongation of the ubiquitin chain in a linkage-specific manner through a single E2 ubiquitin-conjugating enzyme (Ubc2) remains unknown. Here we developed chemical strategies to mimic the reaction intermediates of the first and second ubiquitin transfer steps, and determined the cryo-electron microscopy structures of Ubr1 in complex with Ubc2, ubiquitin and two N-degron peptides, representing the initiation and elongation steps of ubiquitination. Key structural elements, including a Ubc2-binding region and an acceptor ubiquitin-binding loop on Ubr1, were identified and characterized. These structures provide mechanistic insights into the initiation and elongation of ubiquitination catalysed by Ubr1.

Ubiquitination is involved in a wide range of cellular processes³. In particular, the N-degron pathway was the first specific pathway of the ubiquitin (Ub) system to be identified¹. This pathway determines the rate of protein degradation through recognition of the N-terminal residues termed N-degrons. In eukaryotes, N-degrons are recognized by specific Ub ligases (E3), which polyubiquitinate a nearby lysine residue, marking the protein for degradation by the 26S proteasome^{4–6}. It was estimated that more than 80% of human proteins could be regulated by the N-degron pathway⁷. Dysregulation of the N-degron pathway leads to proteotoxicity, which underlies ageing and neurodegeneration⁸.

In *Saccharomyces cerevisiae* (baker's yeast), a single E3 ligase, Ubr1, is responsible for the Arg/N-degron pathway. Ubr1 recognizes two types of N-degrons: type-1 N-degrons start with basic residues and type-2 N-degrons start with bulky hydrophobic residues⁷. Ubr1 is a single-subunit RING-type E3 ligase with a molecular mass of over 200 kDa (Fig. 1a). Despite being discovered over 30 years ago², the molecular structure of Ubr1 is unknown. More importantly, how Ubr1 catalyses the ubiquitination of N-degrons remains to be elucidated.

Ubr1 catalyses Lys48-linked ubiquitination

Previous research has shown that proteins with an Arg/N-degron (43 amino acids) could be polyubiquitinated in vitro by yeast Ubr1 and Ubc2 (also known as Rad6)⁹. We synthesized the degron peptide (Degrон) and a monoubiquitinated version (Ub–Degrон; Extended Data Fig. 1a, b), and reconstituted the polyubiquitination reaction with either peptide as the substrate (Extended Data Fig. 1c–e). When Ub^{K48R} was used instead of wild-type Ub, the polyubiquitination was substantially reduced (Extended Data Fig. 1e). We performed linkage type analyses using a variant of Degrон with a single lysine residue. The results

suggested that Lys48 is the major linkage for the polyubiquitin chain (Extended Data Fig. 2a, b), although a small amount of Lys63-linked diubiquitin was observed when Ub^{K48R} was used (Extended Data Fig. 2c). Single-turnover measurement using Degrон as the substrate showed a Michaelis constant (K_m) and turnover number (K_{cat}) of $1.24 \pm 0.69 \mu\text{M}$ and $0.27 \pm 0.07 \text{ min}^{-1}$, respectively, which represented the initiation step of ubiquitination (Extended Data Fig. 1f). A slightly slower kinetics was observed using Ub–Degrон as the substrate, which represented the first step of Ub chain elongation (Extended Data Fig. 1g). Notably, this behaviour was different from that of multisubunit cullin-RING Ub ligase (CRL), which showed a slow initiation step followed by rapid chain elongation^{10,11}.

The structure of the initiation complex

A stable complex of Ubc2, Ub and Degrон mimicking the reaction intermediate of the initiation step was synthesized (Extended Data Fig. 3a and Supplementary Fig. 1) and mixed with Ubr1, and then analysed using single-particle cryo-electron microscopy (cryo-EM) (Extended Data Fig. 3d and Supplementary Fig. 2a). The final reconstructed map had an overall resolution of 3.35 Å (Extended Data Table 1 and Supplementary Fig. 2b, c). The overall structure of the initiation complex resembled a sailboat (Fig. 1b). The base is a helical scaffold consisting of four regions interspaced by three domains: Ubr-Box1, Ubr-Box2 (also known as the N-domain¹²) and a winged helical domain (WHD) (Fig. 1a and Extended Data Figs. 4a and 5a, b). Similar helical bundle repeats have been observed for other E3 ligases^{13–15}. The structure of Ubr-Box1 has been previously reported^{16,17}. Ubc2 is primarily bound by a single helix of Ubr1, termed the Ubc2-binding region (U2BR, Fig. 1a, b). A RING finger domain follows U2BR and interacts with Ubc2 and the

¹Department of Biochemistry and Molecular Biology, The University of Chicago, Chicago, IL, USA. ²Tsinghua-Peking Center for Life Sciences, Department of Chemistry, Tsinghua University, Beijing, China. ³School of Medicine, Institute of Translational Medicine, Shanghai University, Shanghai, China. ⁴Division of Computing and Software Systems, University of Washington Bothell, Bothell, WA, USA. ⁵These authors contributed equally: Man Pan, Qingyun Zheng, Tian Wang, Lujun Liang.  e-mail: panman@sjtu.edu.cn; yuuy@shu.edu.cn; lliu@mail.tsinghua.edu.cn; mlzhao@uchicago.edu

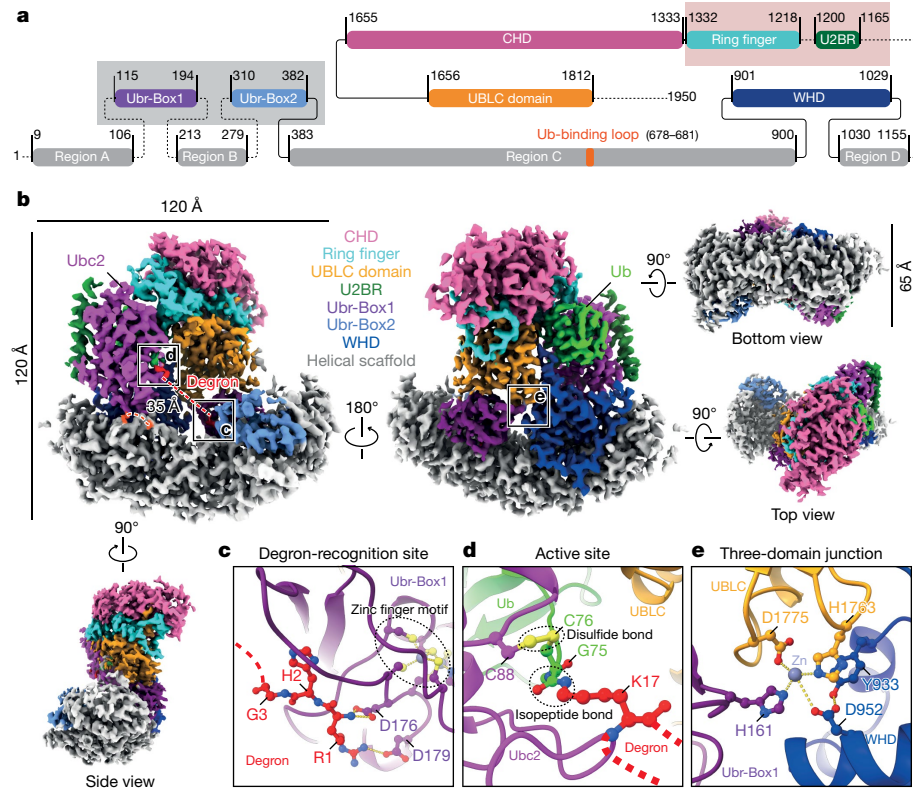


Fig. 1 | The structure of the initiation complex. **a**, Domain diagram of Ubr1; the residue boundaries are indicated. The dotted lines represent unresolved linkers and regions. The grey box indicates the substrate-recruiting domains, and the pink box indicates the Ubc2-recruiting domains. **b**, Cryo-EM maps of the initiation complex (sharpened using a B factor of -96.5 \AA^2 and contoured at a level of 0.030).

The colour code of Ubr1 is the same as in **a**. **c**, Molecular interactions between Degron and Ubr-Box1. Hydrogen bonds and electrostatic interactions are represented by dotted lines. **d**, The molecular structure of the active site. **e**, Molecular interactions between UBLC, Ubr-Box1 and WHD domains. Metal coordination bonds and hydrogen bonds are represented by dotted lines.

loaded Ub (Extended Data Fig. 5d). A previously unidentified domain with a new fold termed the cap helical domain (CHD) follows the RING finger domain (Extended Data Fig. 5c). Finally, the UBR/Leu/Cys (UBLC) domain¹⁸ interacts with Ubr-Box1 and WHD through a putative zinc-binding site (Fig. 1b,e and Extended Data Fig. 4f). Quadruple mutations of the residues involved in this interface (H161A/Y933A/D1175A/H1763A, named DHHY mutant) substantially impaired the activity of Ubr1 (Extended Data Fig. 5g).

The first three residues of the Degron were resolved in the conserved pocket of Ubr-Box1 (ref. ¹⁶) (Fig. 1c and Extended Data Figs. 4d and 6a, b). The recognition was specific as a Met/N-degron could not be polyubiquitinated (Extended Data Fig. 6c). The active site of Ub transfer is around 35 Å away from the C terminus of Gly3, at which Lys17 forms an isopeptide bond with the C-terminal Cys76 of Ub (Fig. 1d and Extended Data Fig. 4e). The residues between Lys17 and Gly3 were not resolved, but the distance indicated an extended conformation (~2.7 Å per residue). Ubr-Box2, homologue of bacterial ClpS^{19–21}, was resolved in our structure. A superimposition of substrate-bound ClpS suggested that a similar mechanism may be adopted by Ubr1 for type-2 N-degrons (Extended Data Fig. 6d–f).

A disulfide bond is formed between Cys76 of the donor Ub and the catalytic residue of Ubc2 (Cys88), as designed (Fig. 1d). The donor Ub is on the back side of the complex and interacts with one of the zinc fingers in the RING finger domain through the Ile36 patch as observed in other E3 complexes^{13,14} (Extended Data Fig. 5d). CHD and WHD also participate in the interaction with the donor Ub (Extended Data Fig. 5e). Polyubiquitination was impaired when mutations of these residues were introduced (Extended Data Fig. 5h). In addition to the interactions with the donor Ub, the U2BR of Ubr1 forms an extensive interface with the

back side of Ubc2 (Fig. 1b), reminiscent of the Ubc2g2-binding region (G2BR) of Gp78 (ref. ²²), and the Ubc7-binding region (U7BR) of Cue1p²³. Together, the non-covalent interactions between Ubr1, Ubc2 and Ub position the Ubc2–Ub thioester bond close to the lysine residue of Degron, facilitating Ub transfer.

The structure of the elongation complex

After the first Ub transfer, subsequent chain elongation requires structural rearrangement. Another stable complex mimicking the transition state of the first elongation step was designed and synthesized (Extended Data Fig. 3b, c and Supplementary Fig. 1), and then analysed using single-particle cryo-EM analyses (Supplementary Fig. 3a). The final reconstructed map had an overall resolution of 3.67 Å (Supplementary Fig. 3b, c), with a similar overall structure to that of the initiation complex (Fig. 2a). The linker molecule covalently linked to Cys88 of Ubc2 forms a disulfide bond with Cys48 of the acceptor Ub and a peptide bond with Gly75 of the donor Ub (Fig. 2b and Extended Data Fig. 4g). The Phe4 patch of the acceptor Ub binds to a loop located in region C of the helical scaffold (termed the Ub-binding loop) (Fig. 2c and Extended Data Fig. 4h), which was disordered in the initiation complex (Fig. 1b). Lys63 is close to this binding interface. Electrostatic interactions with Glu880 and Asp881 may prevent its usage as an acceptor during the elongation reaction (Extended Data Fig. 5f). The acceptor Ub further participated in the recruitment of Ubc2–Ub by binding at a new interface on Ubc2 (Fig. 2d and Extended Data Fig. 4i). When mutations were introduced into the Ub-binding loop of Ubr1 (H678A/V679A/L680A/H681A, named UBLM mutant) and the new interface (Asn123 and Val124 of Ubc2), the polyubiquitination of Degron and Ub–Degron

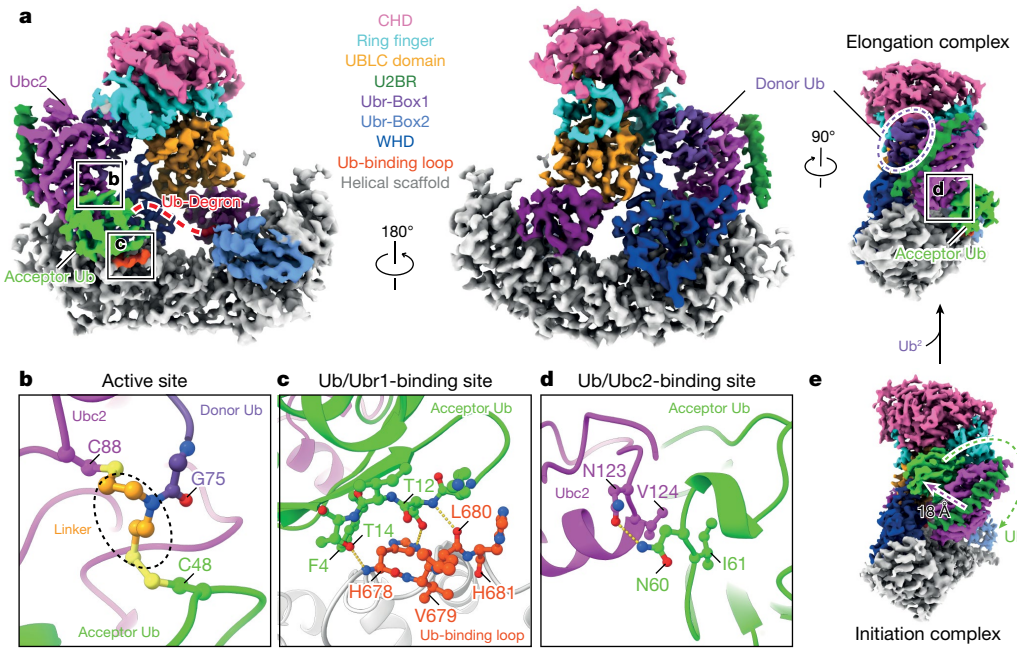


Fig. 2 | The structure of the elongation complex. **a**, Cryo-EM maps of the elongation complex (sharpened using a B factor of -96.7 \AA^2 and contoured at a level of 0.022). The colour code of Ubr1 is the same as in Fig. 1a. **b**, The molecular structure of the active site. **c**, Molecular interactions between the acceptor Ub and the Ub-binding loop of Ubr1. Hydrogen bonds are represented by dotted

lines. **d**, Molecular interactions between the acceptor Ub and Ubc2. Hydrogen bonds are represented by dotted lines. **e**, A side view of the initiation complex in the same orientation as that of the elongation complex in **a**. Displacement of Ubc2, U2BR and Ub is indicated by arrows. The Ub molecules being conjugated are sequentially numbered as Ub^1 , Ub^2 .

was substantially reduced (Extended Data Fig. 7a, b). Notably, the UBLM mutant transferred more Ub to Degron than to Ub–Degron (Extended Data Fig. 7a), and a single-turnover pulse–chase experiment showed that the UBLM mutant failed to transfer fluorescent Ub from Ubc2 to Ub–Degron (Extended Data Fig. 7c), indicating that the Ub-binding loop has a crucial role in the elongation step.

Compared with the initiation complex, U2BR and Ubc2 (including the donor Ub) underwent a displacement of approximately 18 \AA , whereas other domains of Ubr1 remained unchanged (Fig. 2f and Extended Data Fig. 7d, e). This displacement of U2BR and Ubc2 repositioned the presumed thioester bond between Ubc2 and the donor Ub such that this bond was approachable by Lys48 of the acceptor Ub on Ub–Degron (Fig. 2b). Together, the structures of these two complexes suggest that the displacement of U2BR is the key to accommodating extra Ub during the transition from the initiation to the elongation.

Characterization of E2–E3 interfaces

Both complexes showed an extensive binding interface (823.3 \AA^2) between U2BR and Ubc2 (Fig. 3a, b). Mutations of interface residues on U2BR (F1190A/Q1186A/F1183A/H1175A, named FQFH mutant) and Ubc2 severely impaired polyubiquitination (Extended Data Fig. 7f). The presence of a free U2BR peptide (Ubr1^{1165–1200}) inhibited polyubiquitination in a dose-dependent manner due to the competitive binding to Ubc2 (Extended Data Fig. 7g). The dissociation constant (K_d) was $143 \pm 45 \text{ nM}$ as measured by isothermal titration calorimetry (Extended Data Fig. 8a). The formation of E1-dependent thioester bonds (Ubc2–Ub) was inhibited in the presence of the U2BR peptide (Extended Data Fig. 8b, c), which was different from G2BR and U7BR^{22,23}. The accessibility of the catalytic cysteine residue (Cys88) of Ubc2 was decreased in the presence of the U2BR peptide (Extended Data Fig. 7h).

A smaller interface between Ubc2 and the RING finger domain (410.3 \AA^2 for the initiation complex, 208.2 \AA^2 for the elongation complex) was observed compared with previous studies, such as the interface between UbcH5 and the RING finger domain of TRIM25 (547.4 \AA^2)

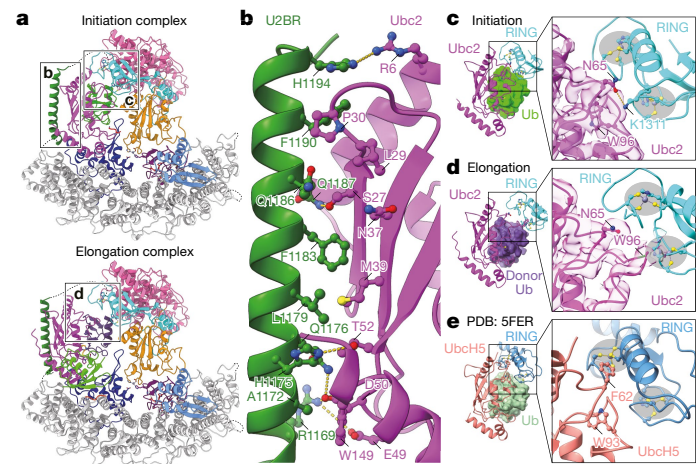


Fig. 3 | Analyses of the interactions between Ubc2 and Ubr1. **a**, The molecular structures of the initiation complex and the elongation complex. **b**, A magnified view of the interface between Ubc2 and U2BR of Ubr1. The labelled residues are involved in extensive noncovalent interactions. Hydrogen bonds and electrostatic interactions are represented by dotted lines. **c–e**, Magnified views of the interface between E2 and RING finger domains. **c**, Ubc2 and the RING finger domain in the initiation complex. Hydrogen bonds are represented by dotted lines. The density of Ubc2 is from the same map in Fig. 1b contoured at a level of 0.030. **d**, Ubc2 and the RING finger domain in the elongation complex. Note that due to the flexibility, the side chains of the loop around Trp96 (green) could not be accurately built into the density. The density of Ubc2 is from the same map in Fig. 2a contoured at a level of 0.020. **e**, UbcH5 and the RING finger domain of TRIM25 (Protein Data Bank (PDB) code 5FER)²⁵.

(Fig. 3c–e)²⁴, although Ubc2–Ub remained in the closed conformation. Sequence alignment showed that Ubc2 has an asparagine residue instead of the conserved phenylalanine residue that is involved

in typical RING–E2 interfaces²⁵ (Extended Data Fig. 7i). Mutating the asparagine back to phenylalanine decreased ubiquitination activity. Interestingly, the N65A mutation increased the amount of polyubiquitinated Degron (Extended Data Fig. 7j), suggesting that Asn65 may not be important for the elongation of the Ub chain. Indeed, in the elongation complex, a loop around the conserved Trp96 underwent conformational changes and interacted with the RING finger domain (Fig. 3d and Extended Data Fig. 7i). Due to the flexibility, the side-chain density of the loop was not well resolved, but it was clear that the interface is altered in the elongation complex and does not resemble the typical RING–E2 interaction that was observed in the closed conformation.

Transition from initiation to elongation

The structural changes from the initiation to the elongation complex require Ubc2 to dissociate from Ubr1 so that the newly conjugated donor Ub can move and act as the new acceptor Ub. To test this hypothesis, catalytically inactive Ubc2 (C88S) or non-hydrolysable Ubc2–Ub²⁶ was premixed with Ubr1 and Degron, and then analysed using a ubiquitination assay with wild-type Ubc2. Minimal inhibitory effects were observed, suggesting that inactive Ubc2 dissociated during the reaction (Extended Data Fig. 8d, e). A complex structure of Ubr1 and Ub–Degron without the presence of Ubc2, named the pre-elongation complex, was determined (Supplementary Fig. 4). The map showed greater flexibility with unresolved U2BR. However, the density corresponding to the acceptor Ub on the Ub-binding loop was clearly identified (Extended Data Fig. 9a), suggesting that the conjugated Ub could bind at the acceptor Ub site in the absence of Ubc2.

Validation of the structural mechanism

We tested several other degron peptides, including an Arg/N-degron derived from human protein Rec8 (^{His}-Type-1 Degron)²⁷ and a type-2 degron peptide derived from Sindbis virus polymerase nsP4 (ref. ²⁸) (Type-2 Degron). Wild-type Ubr1 was able to polyubiquitinate both degrons, whereas mutants of Ubr1 showed decreased activities (Extended Data Fig. 9b, c). Specially, accumulation of monoubiquitinated product in the UBLM mutant was observed, confirming the crucial role of the Ub-binding loop in chain elongation. Furthermore, two truncated native substrates, Scc1^{268–384} (ref. ²⁹) and Roq1^{122–104} (ref. ³⁰), which both contain an N-terminal Arg residue, were tested with similar results (Extended Data Fig. 9d). To validate the structural mechanism in a physiological setting, a previously developed yeast growth assay was performed²⁹ (Extended Data Fig. 9e). The growth defect of $\Delta UBR1$ cells expressing Scc1 was rescued only by co-expressing wild-type Ubr1, and not by co-expressing the Ubr1 mutants, FQFH and UBLM, suggesting that both U2BR and the Ub-binding loop are critical for the Ubr1-dependent N-degron pathway *in vivo* (Extended Data Fig. 9f).

Discussion

Chemical trapping of ubiquitinated intermediates has played critical roles in the mechanistic understanding of various E3 ligases^{13,14,31}. Notably, the structure of Ubr1 alone showed a very flexible CHD and U2BR (Supplementary Fig. 5). After engaging substrates exposing destabilizing N-degrons through the Ubr-Box, and Ub-charged Ubc2 through U2BR and the RING finger domain, Ubr1 facilitates Ub thioester transfer to a Lys residue on the substrate around 40 Å from the N terminus (initiation). Ubc2 is released after the first Ub transfer (pre-elongation). The helical scaffold of Ubr1 provides an anchor (the Ub-binding loop) for the newly conjugated Ub. After the Ub migrates to the new position, it participates in the recruitment of another charged Ubc2 together with the RING finger domain and U2BR, which has shifted to accommodate the acceptor Ub. The interaction between the Ub-binding loop and the acceptor Ub ensures a close proximity of Lys48 to the thioester bond

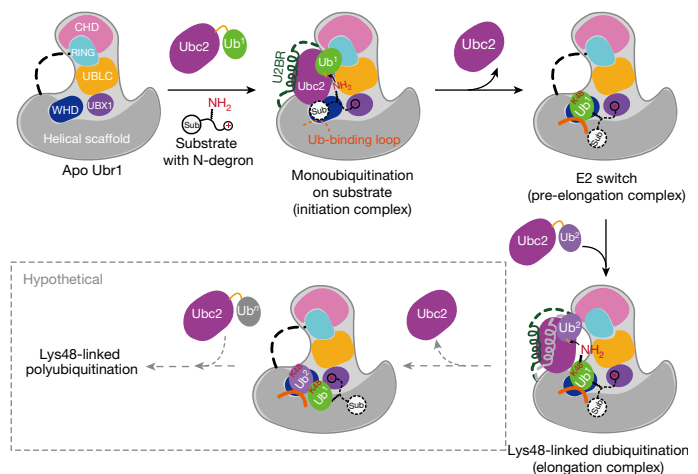


Fig. 4 | A model of Ubr1-mediated polyubiquitination. A cartoon representation of Ubr1-mediated polyubiquitination starting from a degron peptide with a positively charged N-terminal residue (type-1 degron). The first three steps correspond to the initiation, pre-elongation and elongation structures described in this study. Subsequent elongation of the polyubiquitin chain is hypothetical. The Ub molecules being conjugated are sequentially numbered as Ub¹, Ub², Ubⁿ.

of Ubc2–Ub, facilitating the transfer of the second Ub (elongation). We further speculate that similar rearrangements occur for subsequent elongation steps. The most distal acceptor Ub is always engaged by the Ub-binding loop on Ubr1 to ensure the linkage specificity of the polyubiquitin chain (Fig. 4).

Online content

Any methods, additional references, Nature Research reporting summaries, source data, extended data, supplementary information, acknowledgements, peer review information; details of author contributions and competing interests; and statements of data and code availability are available at <https://doi.org/10.1038/s41586-021-04097-8>.

1. Chau, V. et al. A multiubiquitin chain is confined to specific lysine in a targeted short-lived protein. *Science* **243**, 1576–1583 (1989).
2. Bartel, B., Wunning, I. & Varshavsky, A. The recognition component of the N-end rule pathway. *EMBO J.* **9**, 3179–3189 (1990).
3. Komander, D. & Rape, M. The ubiquitin code. *Annu. Rev. Biochem.* **81**, 203–229 (2012).
4. Chen, S. J., Wu, X., Wadas, B., Oh, J. H. & Varshavsky, A. An N-end rule pathway that recognizes proline and destroys gluconeogenic enzymes. *Science* **355**, eaal3655 (2017).
5. Kim, J. M. et al. Formyl-methionine as an N-degron of a eukaryotic N-end rule pathway. *Science* **362**, eaat0174 (2018).
6. Tasaki, T., Sriram, S. M., Park, K. S. & Kwon, Y. T. The N-end rule pathway. *Annu. Rev. Biochem.* **81**, 261–289 (2012).
7. Varshavsky, A. The N-end rule pathway and regulation by proteolysis. *Protein Sci.* **20**, 1298–1345 (2011).
8. Zenker, M. et al. Deficiency of UBR1, a ubiquitin ligase of the N-end rule pathway, causes pancreatic dysfunction, malformations and mental retardation (Johanson-Blizzard syndrome). *Nat. Genet.* **37**, 1345–1350 (2005).
9. Bodnar, N. O. & Rapoport, T. A. Molecular mechanism of substrate processing by the Cdc48 ATPase complex. *Cell* **169**, 722–735 (2017).
10. Petroski, M. D. & Deshaies, R. J. Mechanism of lysine 48-linked ubiquitin-chain synthesis by the cullin-RING ubiquitin-ligase complex SCF-Cdc34. *Cell* **123**, 1107–1120 (2005).
11. Saha, A. & Deshaies, R. J. Multimodal activation of the ubiquitin ligase SCF by Nedd8 conjugation. *Mol. Cell* **32**, 21–31 (2008).
12. Tasaki, T. et al. The substrate recognition domains of the N-end rule pathway. *J. Biol. Chem.* **284**, 1884–1895 (2009).
13. Baek, K. et al. NEDD8 nucleates a multivalent cullin-RING-UBE2D ubiquitin ligation assembly. *Nature* **578**, 461–466 (2020).
14. Horn-Ghetko, D. et al. A Ubiquitin ligation to F-box protein targets by SCF-RBR E3-E3 super-assembly. *Nature* **590**, 671–676 (2021).
15. Rusnak, D. V. & Zheng, N. Structural biology of CRL ubiquitin ligases. *Adv. Exp. Med. Biol.* **1217**, 9–31 (2020).
16. Matta-Camacho, E., Kozlov, G., Li, F. F. & Gehring, K. Structural basis of substrate recognition and specificity in the N-end rule pathway. *Nat. Struct. Mol. Biol.* **17**, 1182–1187 (2010).

17. Choi, W. S. et al. Structural basis for the recognition of N-end rule substrates by the UBR box of ubiquitin ligases. *Nat. Struct. Mol. Biol.* **17**, 1175–1181 (2010).
18. Du, F. Y., Navarro-Garcia, F., Xia, Z. X., Tasaki, T. & Varshavsky, A. Pairs of dipeptides synergistically activate the binding of substrate by ubiquitin ligase through dissociation of its autoinhibitory domain. *Proc. Natl Acad. Sci. USA* **99**, 14110–14115 (2002).
19. Roman-Hernandez, G., Grant, R. A., Sauer, R. T. & Baker, T. A. Molecular basis of substrate selection by the N-end rule adaptor protein ClpS. *Proc. Natl Acad. Sci. USA* **106**, 8888–8893 (2009).
20. AhYoung, A. P., Koehl, A., Vizcarra, C. L., Cascio, D. & Egea, P. F. Structure of a putative ClpS N-end rule adaptor protein from the malaria pathogen *Plasmodium falciparum*. *Protein Sci.* **25**, 689–701 (2016).
21. Kim, L. et al. Structural basis for the N-degron specificity of ClpS1 from *Arabidopsis thaliana*. *Protein Sci.* **30**, 700–708 (2021).
22. Das, R. et al. Allosteric activation of E2-RING finger-mediated ubiquitylation by a structurally defined specific E2-binding region of gp78. *Mol. Cell* **34**, 674–685 (2009).
23. Metzger, M. B. et al. A Structurally unique E2-binding domain activates ubiquitination by the ERAD E2, Ubc7p, through multiple mechanisms. *Mol. Cell* **50**, 516–527 (2013).
24. Koliopoulos, M. G., Esposito, D., Christodoulou, E., Taylor, I. A. & Rittinger, K. Functional role of TRIM E3 ligase oligomerization and regulation of catalytic activity. *EMBO J.* **35**, 1204–1218 (2016).
25. Plechanova, A., Jaffray, E. G., Tatham, M. H., Naismith, J. H. & Hay, R. T. Structure of a RING E3 ligase and ubiquitin-loaded E2 primed for catalysis. *Nature* **489**, 115–120 (2012).
26. Zheng, Q. et al. An E1-catalyzed chemoenzymatic strategy to isopeptide-N-ethylated deubiquitylase-resistant ubiquitin probes. *Angew. Chem. Int. Ed. Engl.* **59**, 13496–13501 (2020).
27. Liu, Y. J. et al. Degradation of the separase-cleaved Rec8, a meiotic cohesin subunit, by the N-end rule pathway. *J. Biol. Chem.* **291**, 7426–7438 (2016).
28. Degroot, R. J., Rumenapf, T., Kuhn, R. J., Strauss, E. G. & Strauss, J. H. Sindbis virus-RNA polymerase is degraded by the N-end rule pathway. *Proc. Natl Acad. Sci. USA* **88**, 8967–8971 (1991).
29. Rao, H., Uhlmann, F., Nasmyth, K. & Varshavsky, A. Degradation of a cohesin subunit by the N-end rule pathway is essential for chromosome stability. *Nature* **410**, 955–959 (2001).
30. Szoradi, T. et al. SHRED is a regulatory cascade that reprograms Ubr1 substrate specificity for enhanced protein quality control during stress. *Mol. Cell* **70**, 1025–1037 (2018).
31. Streich, F. C., Jr & Lima, C. D. Capturing a substrate in an activated RING E3/E2-SUMO complex. *Nature* **536**, 304–308 (2016).

Publisher's note Springer Nature remains neutral with regard to jurisdictional claims in published maps and institutional affiliations.

© The Author(s), under exclusive licence to Springer Nature Limited 2021

Methods

Cloning and plasmid construction

The plasmid containing *S. cerevisiae UBR1* (pFLAG-UBR1-SBX) was obtained from Addgene (plasmid, 24506)³². The DNA sequence of yeast (*S. cerevisiae*) *UBC2* was synthesized and codon-optimized for *Escherichia coli* overexpression by GenScript. The gene was further cloned between the NdeI and Xhol sites of the vector pET-28a containing an N-terminal His tag followed by a HRV3C protease cleavage site. Variants of *UBR1* and *UBC2* were generated using site-directed mutagenesis. Human and yeast *UBA1* were cloned into pET-28a vector containing an N-terminal His tag. DNA sequences encoding wild-type Ub, Ub mutants including K48R, G76C and K0 (all 7 lysine residues mutated to arginine), and AC-Ub (a Ub variant with additional two amino acids Ala-Cys at the N terminus) were synthesized and codon-optimized for *E. coli* overexpression by GenScript. The genes were further cloned between the NdeI and Xhol sites of the vector pET-22b. The truncated *S. cerevisiae* genes *MCD1*(268–384; also known as *SCC1*) and *ROQ1*(22–104; also known as *YJL144W*) were synthesized by GenScript and cloned into the vector pET-28a containing a His-SUMO tag.

Protein expression and purification

Wild-type Ub and Ub mutants were purified as previously described³³. In brief, plasmids for overexpression were transformed into *E. coli* BL21(DE3) competent cells. The *E. coli* cells were grown in Luria broth (LB) medium containing 50 µg ml⁻¹ ampicillin until an optical density at 600 nm (OD₆₀₀) of 0.8, and were then induced by isopropylβ-D-1-thiogalactopyranoside (IPTG) at a final concentration of 0.4 mM followed by overnight incubation at 25 °C. The cells were pelleted at 4,000 r.p.m. for 30 min at 4 °C, resuspended in double-distilled H₂O and lysed by ultrasonication for 30 min in an ice bath. The cell lysates were supplemented with 1% perchloric acid to precipitate non-relevant proteins, which were then cleared using centrifugation (30 min, 15,000g at 4 °C). Ub and its variants were further purified using a Mono S cation exchange column (GE Healthcare), followed by dialysis into a buffer containing 50 mM HEPES, pH 7.5, and 150 mM NaCl. The peak fractions were pooled and concentrated to 20 mg ml⁻¹.

Plasmids containing *UBC2* and its variants were transformed to *E. coli* BL21(DE3) competent cells. The *E. coli* cells were grown in LB medium containing 20 µg ml⁻¹ kanamycin until an OD₆₀₀ of 0.6, and were induced by IPTG at a final concentration of 0.4 mM followed by overnight incubation at 18 °C. The cells were collected by centrifugation at 4,000 r.p.m. for 30 min and then lysed by sonication in the lysis buffer (50 mM HEPES, pH 7.5, 150 mM NaCl, 20 mM imidazole and 1 mM phenylmethyl sulfonyl fluoride (PMSF)). After centrifugation at 12,000 r.p.m. for 30 min, the supernatant was loaded onto a Ni-NTA affinity column. The proteins were eluted with the elution buffer (50 mM HEPES, pH 7.5, 150 mM NaCl and 400 mM imidazole) and further purified by a Superdex 200 size-exclusion column (GE Healthcare) equilibrated in a buffer containing 50 mM HEPES, pH 7.5, and 150 mM NaCl. The expression and purification of Scc1 and Roq1 were performed in a similar manner to that for Ubc2, except that the SUMO protease Ulp1 was used to cleave the soluble SUMO tag and expose the unstable Arg-termini.

Yeast Ubr1 and its variants were expressed as previously described¹⁸. In brief, single colonies of yeast were grown in SD medium at 30 °C until an OD₆₀₀ of around 1.0. The cells were pelleted at 5,000g, washed once with cold phosphate-buffered saline and then resuspended (6 ml buffer per 1 g of pellet) in the lysis buffer (50 mM HEPES, pH 7.5, 0.15 M NaCl, protease inhibitor cocktail (Roche), 1 mM PMSF and 10% glycerol). The resuspended yeast cells were dropped into liquid nitrogen, and the frozen pellet balls were ground into fine powder in liquid nitrogen using a cryogenic impact grinder (SPEX SamplePrep 6870 Freezer/Mill). The powder was further thawed and centrifuged at 11,200g at 4 °C for 30 min. The supernatant was loaded onto anti-DYKDDDDK

(FLAG) affinity resin (Thermo Fisher Scientific, A36803), followed by extensive wash. Finally, the FLAG-tagged Ubr1 was eluted with 1 mg ml⁻¹ Flag peptide and further purified using the Superose 6 size-exclusion column (GE Healthcare) equilibrated in a buffer containing 50 mM HEPES, pH 7.5, and 150 mM NaCl.

Peptide synthesis

All of the peptides were synthesized using standard Fmoc solid-phase peptide synthesis (SPPS) protocols under standard microwave conditions (CEM Liberty Blue). Fmoc-hydrazine 2-chlorotriptyl chloride PS resin and Rink Amide MBHA PS resin were used for peptide synthesis. The coupling cycle was programmed as previously reported³⁴. In brief, 10% piperidine in dimethylformamide with 0.1 M Oxyma (1 min at 90 °C) was applied as deprotection condition, and fourfold of 0.2 M Fmoc-protected amino acid, 1.0 M *N,N*-diisopropylcarbodiimide and 1.0 M Oxyma in dimethylformamide (10 min at 50 °C for His and Cys, 90 °C for other residues) were applied as amino acid coupling conditions. Specifically, in the peptides Ub^{46–76}–K¹⁷Degron-NH₂ and Ub^{48–76}–K¹⁷Degron-NH₂, Fmoc-Lys (Alloc)-OH was coupled at position 17 for the orthogonal protection. When the backbone coupling was finished, the Alloc protecting group was removed by Pd[P(C₆H₅)₃]₄/Ph₃SiH as previously described³⁵, and then the ε-amino group on Lys17 can be further coupled with successive sequence (Ub^{48–76} or Ub^{46–76}). After the completion of SPPS, the resulting peptide resin was cleaved in cleavage cocktail (87% trifluoroacetic acid, 5% water, 5% thioanisole, 3% 1,2-ethanedithiol) for 2 h at 25 °C. Crude peptides were precipitated with cold diethyl ether, analysed and purified by reversed-phase high-performance liquid chromatography (RP-HPLC).

Yeast growth assay

S. cerevisiae strain MAT101 (MATa *LYS2*–801 *URA3*–52 *TRP1*–Δ63 *HIS3*–Δ200 *LEU2*–3,112) lacking *UBR1* (Δ*UBR1*) in the BY4741 background was a gift from R. Hu (University of Chinese Academy of Sciences) (Thermo Fisher Scientific, 95401.H2). The plasmid DHFR–Ub–Arg-Scc1^{269–566} was a gift from H. Rao (Southern University of Science and Technology). DHFR–Ub–Met-Scc1^{269–566} was constructed using standard Quick Change PCR, derived from plasmid DHFR–Ub–Arg-Scc1^{269–566}. Ubr1 mutants (DHHY, UBLM, FQFH) were constructed in the background of the vector Yeplac 181, derived from plasmid 24506 (Addgene) carrying the wild-type *UBR1*.

The following *S. cerevisiae* strains were generated: MAT102 (*UBR1*–*LEU2* in the MAT101 background) and MAT103 (R–Scc1–*URA3* in the MAT101 background) expressing full-length Ubr1 and the R–Scc1^{269–566} fragment from the *P_{GAL1}* promotor; MAT104 (R–Scc1–*URA3*, *UBR1*–*LEU2* in the MAT103 background) and a series of derivative strains (MAT105–107) that express both Ubr1 mutants (DHHY, UBLM or FQFH) and the R–Scc1^{269–566} fragment from the *P_{GAL1}* promotor; and MAT108 (M–Scc1–*URA3* in the MAT102 background) expressing wild-type Ubr1 and the M–Scc1^{269–566} fragment.

Yeast strains described above were grown in rich (YPD) medium containing standard ingredients and 2% glucose. Mid-log-phase yeast cultures (2 ml) were gathered by centrifugation and stored in 2 ml fresh YPD medium containing 50% (v/v) glycerol under –80 °C for further use. Glycerol stocks of different yeast strains (100 µl) were plated onto glucose-containing synthetic media (SD, –Ura, –Leu) plates and grown for 2 d. Single colonies were either plated or spotted in serial tenfold dilution onto the SD (–Ura, –Leu) and SG (containing 2% galactose rather than glucose, –Ura, –Leu) plates. The plates were incubated for 3 d before imaging.

Preparation of fluorescently labelled Degron and Ub–Degron

Degron was directly obtained from SPPS as described above. K17-linked mono-ubiquitinated Degron (Ub–K¹⁷Degron) was synthesized from two fragments, Ub^{1–45}–NH₂ and Ub^{46–76}–K¹⁷Degron–NH₂. Ala46 in the latter fragment was temporally mutated to Cys to enable native chemical

ligation of these two fragments. After ligation the thiol group of Cys46 was removed through desulfurization reaction to produce the native Ala46 as shown in Supplementary Fig. 1b. For fluorescence labelling of Degron, we introduced an additional Cys at the C terminus of Degron to enable site-specific labelling. In the case of Ub–Degron, a Cys(Acm) was introduced into the C terminus of Degron to orthogonally protect this thiol group from being desulfurized. After purification, the Acm group was removed from the Ub–Degron–Cys(Acm) to obtain a free thiol group. For the labelling reaction, 2 mg lyophilized dry powder of Degron–Cys or Ub–Degron–Cys was dissolved in 50 mM HEPES, 150 mM NaCl, pH 7.5. Then, 2 eq. of fluorescein-5-maleimide (Invitrogen, F150) was added and the mixture was incubated at room temperature for 20 min, followed by buffer exchange in 50 mM HEPES, 150 mM NaCl (pH 7.5) using a Superdex peptide size-exclusion column (GE Healthcare) to give the fluorescently labelled Degron and Ub–Degron.

Ubiquitination assay with fluorescent Degron or Ub–Degron

In vitro ubiquitination assays were performed with 0.1 μ M Uba1, 4 μ M Ubc2, 0.25 μ M Ubr1, 5 μ M fluorescent Degron or Ub–Degron, and 80 μ M Ub at 30 °C in the reaction buffer (50 mM HEPES, pH 7.5, 0.15 M NaCl, 10 mM MgCl₂ and 5 mM ATP). The reactions were terminated by adding 4 \times sodium dodecyl sulfate (SDS) sample buffer, and then analysed using SDS–polyacrylamide gel electrophoresis (PAGE). Unless indicated otherwise, the same concentrations of Ubr1 and Ubc2 variants were used in the assay as the respective wild type.

Single-turnover measurement of Ub transfer in the initiation and elongation steps

To monitor the single-turnover of Ub transfer in the initiation step, that is, Ubr1 transfers Ubc2–Ub to Degron, a pulse–chase experiment that eliminates the effects of UBA1-dependent formation of Ubc2–Ub intermediate was performed. The pulse reaction generated a thioester-linked Ubc2–Ub intermediate with 5 μ M Ubc2, 7.5 μ M fluorescent Ub, 0.5 μ M UBA1 in a buffer containing 50 mM HEPES pH 8.0, 150 mM NaCl, 2 mM MgCl₂ and 2 mM ATP. The reaction mixture was incubated at room temperature for 10 min, and quenched with 50 mM EDTA on ice for 5 min. A final concentration of 0.5 μ M Ubr1 and 25 μ M unlabelled Degron was added for the chase reaction, which was then incubated at 30 °C for 5 min. The reaction was stopped by adding 2 \times SDS sample buffer (pH < 3), and then analysed using SDS–PAGE. The same concentrations of Ubr1 and Ubc2 variants were used as the respective wild type. The experimental set-up for the elongation step was similar to the initiation step, except that fluorescently labelled Ub–Degron was used instead of Degron.

K_m measurement of the initiation and elongation steps

For K_m measurement of the initiation step, two prepared mixtures are required. Mixture 1 consists of UBA1 and Ub^{K48R}, and mixture 2 consists of Ubr1 and fluorescently labelled Degron. Both mixtures were prepared in the reaction buffer (50 mM HEPES, pH 7.5, 150 mM NaCl, 10 mM MgCl₂ and 5 mM ATP). Ubc2 was prepared as a twofold dilution series from the stock, and then introduced into the solution containing equal amounts of the two mixtures to initiate the reaction. The final concentrations were 80 μ M Ub^{K48R}, 0.1 μ M Uba1, 0.25 μ M Ubr1 and 5 μ M fluorescently labelled Degron. The reactions were quenched after 1 min at 30 °C using 2 \times SDS sample buffer, and then analysed using SDS–PAGE. The gels were imaged on ChemiDoc MP Imaging System. Substrate and product bands were individually quantified as the percentage of the total signal for each time point using ImageLab (Bio-Rad). Ratios of ubiquitinated products relative to the total signal were plotted against the concentration of Ubc2 and fitted to the Michaelis–Menten equation to estimate K_m in GraphPad Prism v.8.2.1. The experimental setup for the K_m measurement of the elongation step was similar, except that fluorescently labelled Ub–Degron was used instead of Degron.

Generation of the stable complex mimicking the transition state of the initiation step

Preparation of Ub^{1–75} hydrazide. Ub^{1–75} hydrazide (Ub75–NHNH₂) was generated using previously reported protein hydrazinolysis method³³. In brief, Ub^{G76C} of which Gly76 at the C terminus was mutated to Cys could undergo N-S acyl transfer such that hydrazine could be used as a suitable nucleophile, leading to a reliable C-terminal hydrazinolysis. Then, 20 mg ml^{–1} Ub^{G76C}, 5 mg ml^{–1} tris(2-carboxyethyl) phosphine (TCEP), 50 mg ml^{–1} NHNH₂·HCl and 100 mg ml^{–1} sodium 2-mercaptopethanesulfonate (MesNa) were mixed in 20 mM Tris, pH 6.5, and stirred at 60 r.p.m. and 50 °C for 24 h. The final products were analysed and purified using RP-HPLC.

Preparation of Ub^{G76C–K17} Degron. The reaction scheme is shown in Supplementary Fig. 6a. In brief, Ub75–NHNH₂ peptide (1 μ mol, 1 eq.) was dissolved in 1 ml ligation buffer (6 M guanidinium chloride, 100 mM NaH₂PO₄, pH 2.3) precooled to –15 °C. Then, 10 μ l 1 M NaNO₂ (10 μ mol, 10 eq.) was added, and the reaction was stirred for 30 min at –15 °C to fully convert the hydrazide to the acyl azide. Next, MesNa (100 μ mol, 100 eq.) was added, and the pH was adjusted to 5.0 for overnight reaction. The product, Ub^{1–75}–MesNa, was further purified by RP-HPLC. Purified Ub^{1–75}–MesNa (1 μ mol, 1 eq.) and Cys^{K17}–Degron peptide (1.1 μ mol, 1.1 eq.) were mixed with the ligation buffer (6 M guanidinium chloride, 100 mM NaH₂PO₄, 5 mg ml^{–1} TCEP, pH 7.4). Next, 4-mercaptophenylacetic acid (MPAA, 50 μ mol, 50 eq.) was added, and the pH was adjusted to 6.4 for overnight reaction. The final product Ub^{G76C–K17}–Degron was analysed and purified using RP-HPLC.

Preparation of Ubc2–Ub^{G76C–K17} Degron through disulfide ligation. Lyophilized dry powder of Ub^{G76C–K17}–Degron (1.3 mg) was dissolved in 100 μ l 6 M guanidinium chloride, 50 mM HEPES, pH 7.5, to a final concentration of 1 mM. Then, 2 μ l of 100 mM 5,5'-dithiobis-(2-nitrobenzoic acid) (Sigma Aldrich; dissolved in 50 mM NaH₂PO₄, pH 7.5) was immediately added and fully mixed by pipetting before incubating at room temperature for 20 min. The solution was then diluted to the refolding buffer containing 50 mM HEPES pH 7.5, 150 mM NaCl. Excess reactants were removed using the Superdex peptide size-exclusion column (GE Healthcare) equilibrated in the refolding buffer. Finally, the product and 0.9 eq. Ubc2 (predialysed into the refolding buffer) were mixed and incubated at room temperature for 30 min. The final product was analysed and purified using RP-HPLC.

Generation of the stable complex mimicking the transition state of the elongation step

Preparation of molecule 2. As shown in Extended Data Fig. 3c, molecule **2** was prepared using Cys-aminoethylation reaction²⁶. Specifically, 1 μ mol lyophilized powder of Ubc2 was incubated in aqueous alkylation buffer (6 M guanidinium chloride, 0.1 M HEPES, pH 8.5, 5 mg ml^{–1} TCEP) with 40 mM molecule **1** (2-((2-chloroethyl)amino)ethane-1-(S-acetaminomethyl)thiol) at 37 °C for 14–16 h. The product, molecule **2**, was further purified by semi-preparative HPLC and lyophilized.

Preparation of molecule 3. Lyophilized molecule **2** was dissolved in reaction buffer containing 6 M guanidinium chloride, 0.1 M NaH₂PO₄ buffer, pH 7.4 at a final concentration of 1 mM. Then, PdCl₂ (15 eq., pre-dissolved in the reaction buffer) was added and the mixture was incubated at 37 °C for 1 h to remove the Acm group. Purified Ub^{1–75}–MesNa was then added and mixed in the ligation buffer (6 M guanidinium chloride, 0.1 M NaH₂PO₄, 5 mg ml^{–1} TCEP, pH 7.4) at a final concentration of 1.1 mM (1.1 eq.). Next, MPAA (150 μ mol, 150 eq.) was added, and the pH was adjusted to 6.4 to initiate native chemical ligation (Extended Data Fig. 3c). The product was analysed and purified using RP-HPLC.

Preparation of Ub^{K48C-K17}Degron. Different from the preparation strategy for Ub–Degron, we mutated the Lys48 to Cys, which enabled native chemical ligation. Furthermore, the thiol group on Cys48 was retained for disulfide ligation. Specifically, Ub¹⁻⁴⁷NHNH₂ peptide (1 µmol, 1 eq.) was dissolved in 1 ml ligation buffer (6 M guanidinium chloride, 100 mM NaH₂PO₄, pH 2.3) precooled to –15 °C. Then, 10 µl 1 M NaNO₂ (10 µmol, 10 eq.) was added, and the reaction was stirred for 30 min at –15 °C to fully convert the hydrazide to acyl azide. Next, Ub^{48-76/K48C-K17}Degron peptide (1.1 µmol, 1.1 eq.) was added to the ligation buffer, followed by MPAA (50 µmol, 50 eq.). The pH was adjusted to 6.4 to initiate the ligation (Supplementary Fig. 6b). The product, Ub^{K48C-K17}Degron, was analysed and purified using RP-HPLC.

Preparation of Ubc2–Ub–Ub^{K48C-K17}Degron using disulfide ligation. Lyophilized dry powder of molecule 3 was dissolved in 500 µl 6 M guanidinium chloride, 50 mM HEPES and 1 mM TCEP, pH 7.5, and refolded through gradient dialysis against refolding buffer (50 mM HEPES, 1 mM TCEP, pH 7.5) containing 6 M, 2 M, 1 M to 0 M guanidinium chloride. Then, 1.3 mg lyophilized dry powder Ub^{K48C-K17}Degron was dissolved in 100 µl 6 M guanidinium chloride, 50 mM HEPES, pH 7.5 (the final concentration was 1 mM), and then 2 µl 100 mM 5,5'-dithiobis-(2-nitrobenzoic acid) (Sigma Aldrich, dissolved in 50 mM NaH₂PO₄, pH 7.5) was added and fully mixed by pipetting before incubating at room temperature for 20 min. The solution was then diluted to the refolding buffer, and the excess small molecule was removed using the Superdex peptide size-exclusion column (GE Healthcare) equilibrated in refolding buffer. Finally, the pooled product and 1.1 eq. refolded molecular 3 were mixed and incubated at room temperature for 30 min. The final product, Ubc2–Ub–Ub^{K48C-K17}Degron, was analysed and purified using RP-HPLC.

Sample preparation for single-particle cryo-EM

Ubr1 (0.4 mg ml^{–1}) was mixed with 1.5-fold excess (molar ratio) initiation, or elongation intermediate mimics and incubated on ice for 30 min. For the pre-elongation complex, Ubr1 was mixed with 1.5-fold Ub–Degron on ice for 30 min. A final concentration of 0.01% fluorinated octyl maltoside was added to the sample immediately before grid-freezing using a Vitrobot mark IV (Thermo Fisher Scientific) operating at 8 °C and 100% humidity. A volume of 3.5 µl sample was applied to a glow-discharged Quantifoil Cu 1.2/1.3 grid, and blotted for 1 s using standard Vitrobot filter paper (Ted Pella, 47000-100) before plunge-freezing into liquid ethane.

Data collection for single-particle cryo-EM

Optimized frozen grids were sent to the Advanced Electron Microscopy Facility at the University of Chicago or National Cryo-Electron Microscopy Facility at National Cancer Institute for data collection. All datasets were acquired as video stacks using a Titan Krios electron microscope (Thermo Fisher Scientific) operating at 300 kV, equipped with a Gatan K3 direct detection camera. A single stack consists of 40 frames with a total exposure around 50 electrons per Å². The defocus range was set at –1.0 µm to –2.5 µm (details are provided in Extended Data Table 1).

Image processing

Video stacks were processed for motion correction using MotionCor2 (v.1.3.2)³⁶. Contrast transfer function parameters for each micrograph were determined using CTFFIND4 (v.4.1.9)³⁷. The following particle picking, two-dimensional (2D) and three-dimensional (3D) classifications, and 3D refinement were performed in RELION-3.1 (ref. ³⁸). About 2,000 particles were manually picked to generate 2D class averages. The class averages were then used as templates for the following automatic particle picking. False-positive particles or particles classified in poorly defined classes were discarded after 2D classification. Initial 3D classification was performed on a binned dataset using the initial model

obtained in RELION. The detailed data processing flows are shown in Supplementary Figs. 2 and 4–6. Only small fractions of particles went into the final 3D reconstruction, which may result from several factors. First, as many particles as reasonable were picked at the beginning to account for rare orientations. Second, the efficiency of complex formation may affect the number of useful particles. Finally, other factors such as the air–water interface and the detergent used to fix the orientation preference may also contribute to the small percentage of particles that went into the final 3D reconstruction. Data processing statistics are summarized in Extended Data Table 1. Reported resolutions are based on Fourier shell correlation (FSC) using the FSC = 0.143 criterion. Local resolution was determined using the implementation in RELION.

Model building, refinement and validation

Yeast Ubr1 is a single-subunit E3 comprising 1,950 amino acids. Only the structure of Ubr-Box1 domain was determined previously^{16,17}. The artificial-intelligence-based de novo modelling tool DeepTracer³⁹ was used to build a starting model of the entire complex from scratch. Specifically, the sharpened map of the initiation complex and a FASTA file containing sequences of Ubr1, Ubc2 and Ub were input into the online server of DeepTracer (<https://deeptracer.uw.edu/home>). The program output a complete model with Ubc2 and Ub correctly positioned. About 80% of Ubr1 was correctly built into the cryo-EM map, with some errors in the poorly resolved regions and the zinc-binding sites. The starting model was first refined in real space using PHENIX (v.1.15.2)⁴⁰, and then manually fixed, adjusted and refined using COOT⁴¹. About 1,800 residues of Ubr1 were built except for some flexible loops and around 140 C-terminal residues. The registration of the main chain was carefully checked and fixed based on bulky residues. The entire procedure was greatly simplified and accelerated with the starting model from DeepTracer. To further improve the geometry of the atomic models, ISOLDE⁴² embedded in ChimeraX (v.0.9)⁴³ was used to fix most rotamer and Ramachandran outliers. Multiple rounds of manual model building/optimization in COOT (v.0.89) and ISOLDE followed by PHENIX real space refinement were performed. Both sharpened and unsharpened maps were used. The unsharpened maps were used in the earlier iterations. Sharpened maps were used for the final refinement as they have better-resolved side-chain density. The resolution of the elongation complex was worse, but some loop areas were better resolved and were used to aid the modelling of the initiation complex. Tetrahedral geometry restraints of the zinc-binding sites were applied wherever reasonable. The following strategies have been tried to improve the fitting of the chemical linker in the elongation complex, including changing the expected sigma of customized restraints and applying higher weight on the experimental data during the refinement. Owing to the flexibility of the chemical linker, the density around the linker including a loop containing Trp96 of Ubc2 in the elongation complex was not resolved as well as the rest of the map. Special attention was paid to model interpretation. The statistics of model refinement and geometry are shown in Extended Data Table 1. Molecular graphics and analyses were performed using UCSF ChimeraX⁴³ and PISA at the European Bioinformatics Institute (http://www.ebi.ac.uk/pdbe/prot_int/pistart.html)⁴⁴. Structure comparison and domain identification were performed using the DALI server for protein structure comparison⁴⁵ and SWISS-MODEL⁴⁶.

Ubc2–Ub thioester formation in the presence of U2BR peptide

First, 0.5 µM Uba1, 5 µM Ubc2 and 7.5 µM fluorescently labelled Ub were mixed in the reaction buffer containing 50 mM HEPES pH 8.0 and 150 mM NaCl. U2BR peptide was prepared as a twofold dilution series from the stock and added to the reaction mixture. Prepared ATP-Mg²⁺ mixture (50 mM MgCl₂, 50 mM ATP, pH 8.0) was added to initiate the Ubc2–Ub thioester formation. Reactions were quenched after 10 min at 30 °C using 2× SDS sample buffer (pH < 3), and then analysed using SDS-PAGE. The gels were imaged on the ChemiDoc MP Imaging System,

Article

and substrate and product bands were quantified as a percentage of the total signal for each time point using ImageLab (Bio-Rad). The ratio of ubiquitylated products relative to the total signal was plotted against the concentrations of Ubc2 and fitted to the inhibitor-versus-response model (three parameters) in GraphPad Prism 8.

Isothermal titration calorimetry analysis

All reported isothermal titration calorimetry data were collected using a MicroCal ITC 200 instrument in the Centre of Biomedical Analysis, Tsinghua University. Ubc2 and all U2BR peptides were buffer-exchanged into 50 mM HEPES, pH 7.5, and 150 mM NaCl before the experiment. For the experiments, 20 μ M Ubc2 solution in the sample cell was titrated with 200 μ M U2BR peptide solution through 19 injections (2.0 μ l each) at 25 °C and 750 r.p.m. stirring speed. Data fitting and analyses were performed using Origin 7 SR4 (OriginLab).

Reporting summary

Further information on research design is available in the Nature Research Reporting Summary linked to this paper.

Data availability

Cryo-EM maps have been deposited in the Electron Microscopy Data Bank (EMDB, www.ebi.ac.uk/pdbe/emdb/) under accession codes EMDB-23806 (initiation complex), EMDB-23807 (elongation complex), EMDB-24935 (pre-elongation complex) and EMDB-24936 (apo Ubr1). The atomic models have been deposited in the Protein Data Bank (PDB, www.rcsb.org) under the accession codes 7MEX (initiation complex) and 7MEY (elongation complex). The atomic model of UbcH5 and the RING finger domain of TRIM25 is available under PDB accession code 5FER. Uncropped gels and blots source data are provided in Supplementary Fig. 7. Owing to the large file size, raw electron microscopy data are available from the corresponding authors on request. Source data are provided with this paper.

32. Xia, Z. et al. Substrate-binding sites of UBR1, the ubiquitin ligase of the N-end rule pathway. *J. Biol. Chem.* **283**, 24011–24028 (2008).
33. Pan, M. et al. Chemical protein synthesis enabled mechanistic studies on the molecular recognition of K27-linked ubiquitin chains. *Angew. Chem. Int. Ed. Engl.* **58**, 2627–2631 (2019).
34. Pan, M. et al. Quasi-racemic X-ray structures of K27-linked ubiquitin chains prepared by total chemical synthesis. *J. Am. Chem. Soc.* **138**, 7429–7435 (2016).
35. Qu, Q. et al. A highly efficient synthesis of polyubiquitin chains. *Adv. Sci.* **5**, 1800234 (2018).
36. Zheng, S. Q. et al. MotionCor2: anisotropic correction of beam-induced motion for improved cryo-electron microscopy. *Nat. Methods* **14**, 331–332 (2017).
37. Mindell, J. A. & Grigorieff, N. Accurate determination of local defocus and specimen tilt in electron microscopy. *J. Struct. Biol.* **142**, 334–347 (2003).
38. Zivanov, J. et al. New tools for automated high-resolution cryo-EM structure determination in RELION-3. *eLife* **7**, e42166 (2018).

39. Pfab, J., Phan, N. M. & Si, D. DeepTracer for fast de novo cryo-EM protein structure modeling and special studies on CoV-related complexes. *Proc. Natl. Acad. Sci. USA* **118**, e2017525118 (2021).
40. Adams, P. D. et al. PHENIX: a comprehensive Python-based system for macromolecular structure solution. *Acta. Crystallogr. D* **66**, 213–221 (2010).
41. Emsley, P. & Cowtan, K. Coot: model-building tools for molecular graphics. *Acta. Crystallogr. D* **60**, 2126–2132 (2004).
42. Croll, T. I. ISOLDE: a physically realistic environment for model building into low-resolution electron-density maps. *Acta Crystallogr. D* **74**, 519–530 (2018).
43. Pettersen, E. F. et al. UCSF ChimeraX: structure visualization for researchers, educators, and developers. *Protein Sci.* **30**, 70–82 (2021).
44. Krissinel, E. & Henrick, K. Inference of macromolecular assemblies from crystalline state. *J. Mol. Biol.* **372**, 774–797 (2007).
45. Holm, L. DALI and the persistence of protein shape. *Protein Sci.* **29**, 128–140 (2020).
46. Waterhouse, A. et al. SWISS-MODEL: homology modelling of protein structures and complexes. *Nucleic Acids Res.* **46**, W296–W303 (2018).

Acknowledgements We thank the staff at the National Cryo-Electron Microscopy Facility at the Frederick National Laboratory and the Advanced Electron Microscopy Facility at the University of Chicago for the help with cryo-EM data collection; H. Rao (Southern University of Science and Technology) and R. Hu (University of Chinese Academy of Sciences) for their help in yeast related experiments. Funding for this work was in part provided by the Catalyst Award C-086 to M.Z. from the Chicago Biomedical Consortium. M.Z. is supported by National Institute of General Medical Sciences of the National Institutes of Health (NIH) under award number R35GM143052. We thank the National Key R&D Program of China (no. 2017YFA0505200) and NSFC (nos 91753205, 81621002, 21621003) for financial support; the National Postdoctoral Program for Innovative Talents (BX2021143), Shuimu Tsinghua Scholar Program (2021SM067) for financial support. This research was in part supported by the National Cancer Institute's National Cryo-EM Facility at the Frederick National Laboratory for Cancer Research under contract HSSN261200800001E. This research is based on work supported by the National Science Foundation under grant no. 2030381, the graduate research award of Computing and Software Systems division and the start-up fund 74-0525 at University of Washington Bothell to D.S. Any opinions, findings, and conclusions or recommendations expressed in this paper are those of the authors and do not necessarily reflect the views of the National Science Foundation. Molecular graphics and analyses were performed using UCSF ChimeraX, developed by the Resource for Biocomputing, Visualization, and Informatics at the University of California, San Francisco, with support from NIH R01GM129325 and the Office of Cyber Infrastructure and Computational Biology, National Institute of Allergy and Infectious Diseases.

Author contributions M.P., M.Z., L. Liu and Y.Y. designed all of the experiments and interpreted the results. M.P., Q.Z. and L. Liu designed the synthetic route for chemically synthesized ubiquitination initiation and elongation intermediate mimics. T.W. synthesized the fluorescently labelled Ub-Degron and the elongation intermediate mimic. L. Liang synthesized the fluorescently labelled Degron and the initiation intermediate mimic. M.P., Y.Y., D.S. and M.Z. performed cryo-EM data collection and processing. J.M. performed the in vitro ubiquitination assays with Ubr1 and Ubc2 mutants. Q.Z. performed characterization of the U2BR peptide on the enzymatic properties of Ubc2. T.W., Y.Y., C.Z., R.D., J.M., H.A. and Y.X. cloned, expressed and purified Ubr1, Ubc2 and their mutants. M.Z., M.P. and L. Liu wrote the paper. M.Z., L. Liu, Y.Y. and M.P. supervised the project.

Competing interests The authors declare no competing interests.

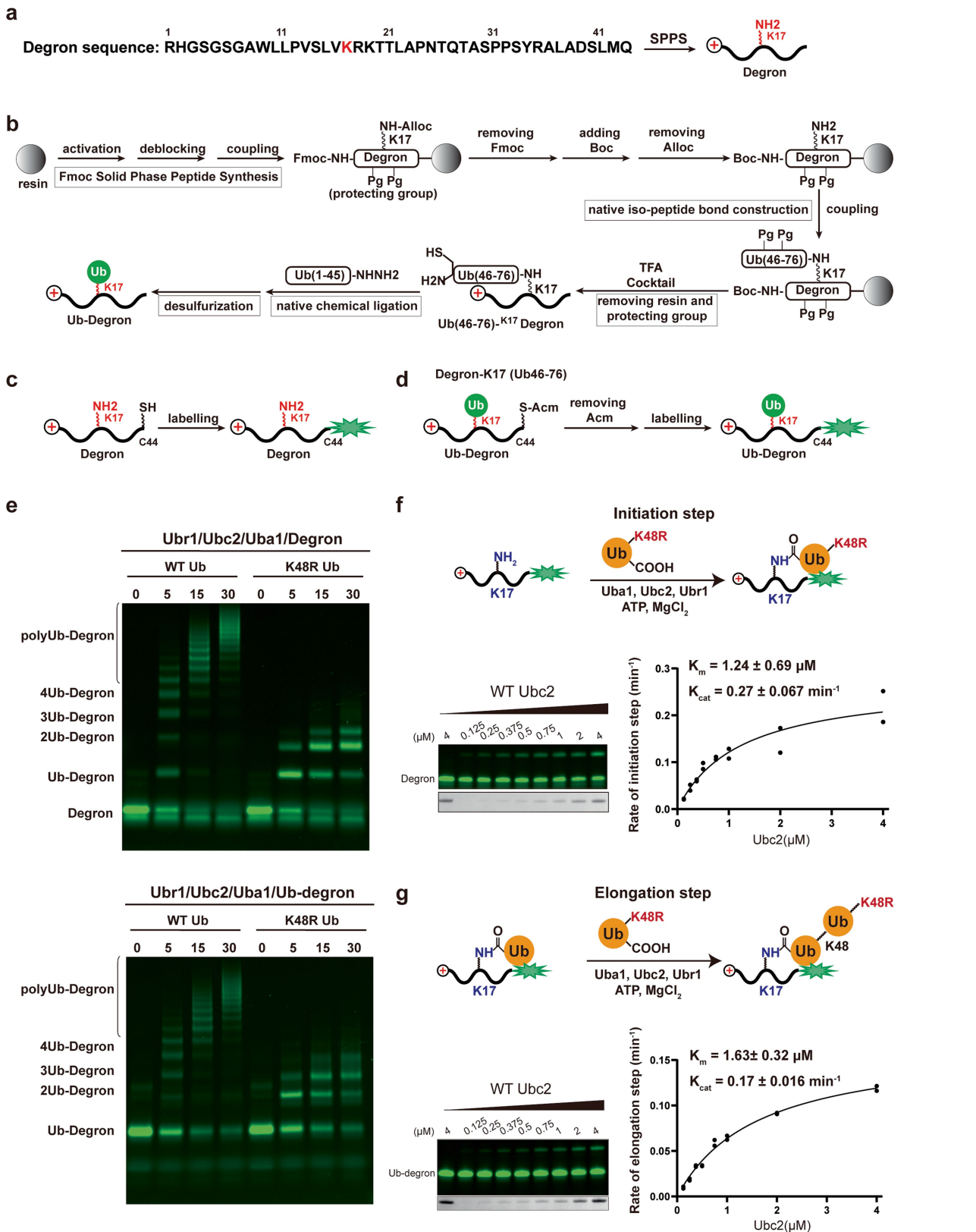
Additional information

Supplementary information The online version contains supplementary material available at <https://doi.org/10.1038/s41586-021-04097-8>.

Correspondence and requests for materials should be addressed to Man Pan, Yuanyuan Yu, Lei Liu or Minglei Zhao.

Peer review information *Nature* thanks Yong Tae Kwon and the other, anonymous, reviewer(s) for their contribution to the peer review of this work. Peer reviewer reports are available.

Reprints and permissions information is available at <http://www.nature.com/reprints>.



Extended Data Fig. 1 | Ubr1-mediated Lys48-linked polyubiquitination of degron peptides. **a**, The amino acid sequence of the degron peptide (Degron). SPPS: solid-phase peptide synthesis. **b**, The synthetic route of the monoubiquitinated degron peptide (Ub-Degron). **c-d**, Fluorescent labelling of Degron (**c**) and Ub-Degron (**d**). An additional C-terminal cysteine was introduced for the labelling of fluorescein-5-maleimide. **e**, In vitro Ubr1-dependent ubiquitination assays using fluorescent Degron (top) and

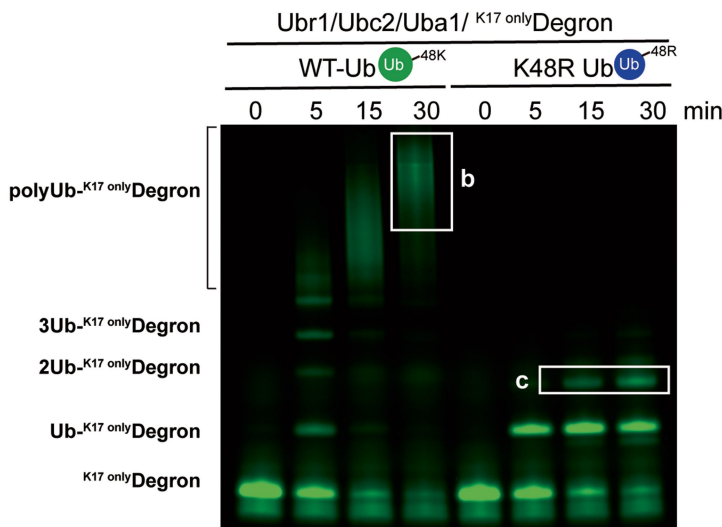
Ub-Degron (bottom) as substrates. Gel images are representative of independent biological replicates ($n=2$). **f-g**, Quantitative evaluations of the kinetics of Ubr1-mediated ubiquitination initiation (**f**) and the first step of elongation (**g**). Averages of two independent experiments were plotted and fitted to the Michaelis–Menten model to estimate the K_m and K_{cat} . Gel images are representative of independent biological replicates ($n=2$).

Article

a

K17 only Degron:

RHGSGSGAWLLPVSLV**KRR**TTLAPNTQTASPPSYRALADSLMQ



b

MS-MS Result of polyUb-^{K17 only}Deqon using WT Ub

Linkage type	Ubiquitin sequence	# PSMs	Modifications	Area
K48	LIFAG k QLEDGR	100	K6(GlyGly)	1.848E11
K48	LIFAG k QLEDGRTLSNDYNIQK	14	K6(GlyGly)	4.196E9
K63	TLSNDYNIQ k ESTLHLVLR	17	K9(GlyGly)	1.451E10
K63	TLSNDYNIQ k ESTLHLVLRLLR	5	K9(GlyGly)	1.252E9
K11	TLTG k TITLEVEPSDTIENVK	8	K5(GlyGly)	7.329E9
K33	IQD k EGIPPDQQR	4	K4(GlyGly)	2.763E8
K6	mQIFV k TLTGK	1	M1(Oxidation); K6(GlyGly)	1.096E8
K6	MQIFV k TLTGK	1	K6(GlyGly)	7.091E7

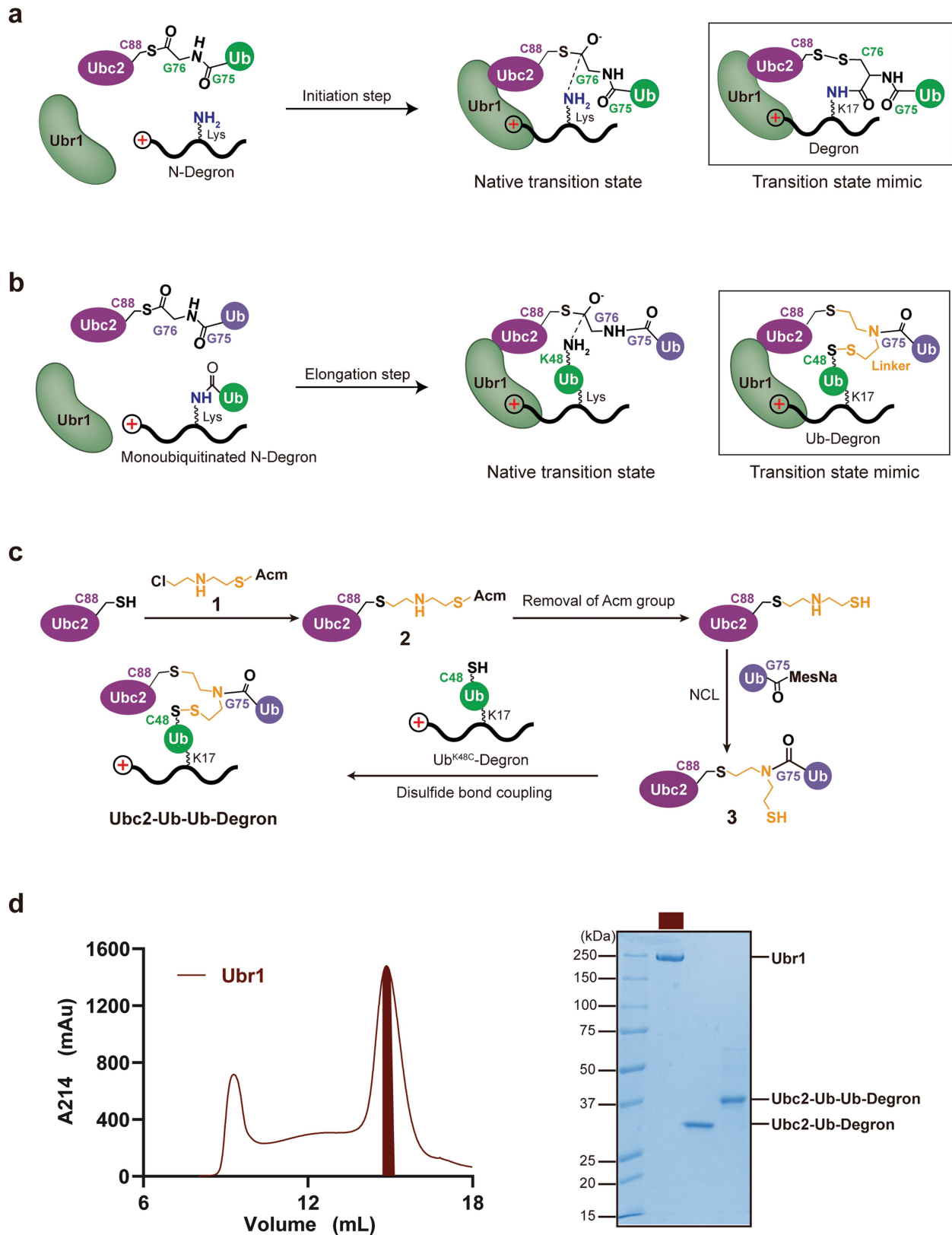
C

MS-MS Result of diUb-K17 only Degon using K48R Ub

Linkage type	Ubiquitin sequence	# PSMs	Modifications	Area
K63	TLSVDYNIQKESTLHLVLR	13	K9(GlyGly)	2.884E9

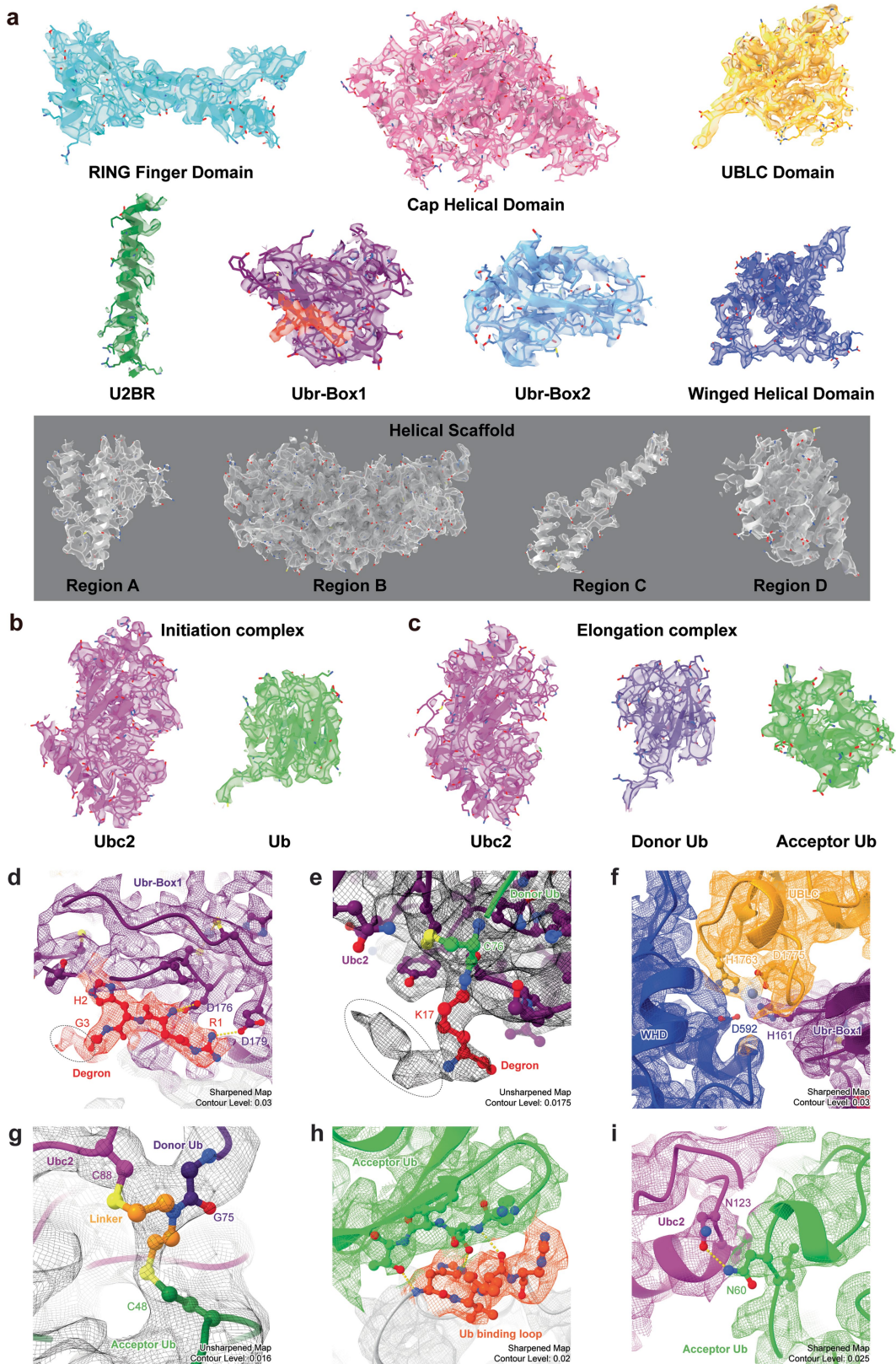
Extended Data Fig. 2 | Analyses of ubiquitin chain linkage generated by Ubr1 and Ubc2. **a**, *In vitro* Ubr1-dependent ubiquitination on fluorescently labelled K17onlyDegrон using wild-type Ub (left) and Ub^{K48R} (right). Gel images are representative of independent biological replicates ($n=2$). Gel slices in box

b and **c** were cut and digested, followed by LC-MS/MS analyses. **b**, Identification of Ub chain linkages in box b. **c**, Identification of Ub chain linkages in box c. #PSMs: Number of peptide spectrum matches.



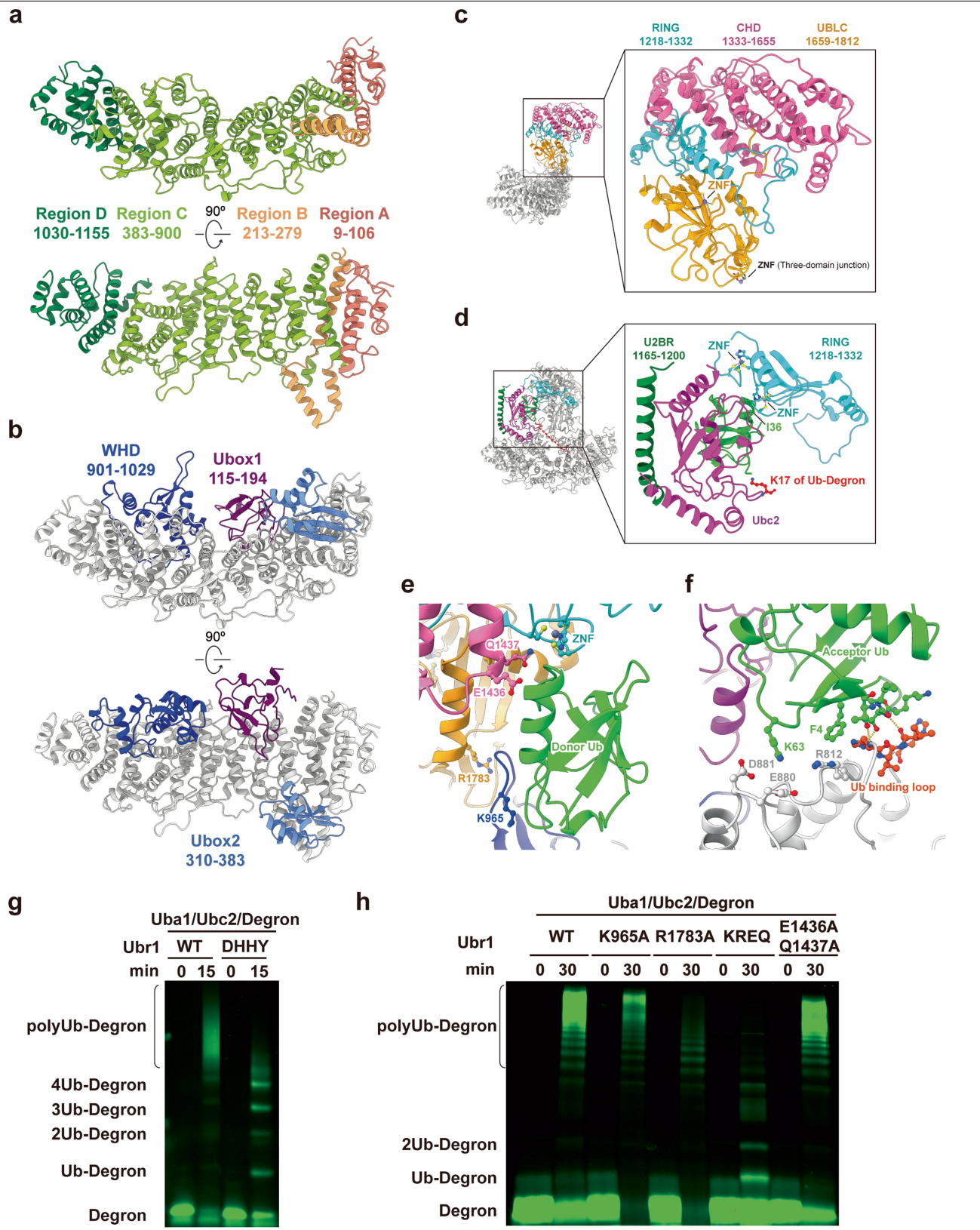
Extended Data Fig. 3 | Design and purification of the stable intermediate structures. **a**, A schematic representation of the transition state of the initiation step. The side chain of a Lys residue on Degron attacks the thioester bond of Ubc2-Ub. The inset shows the designed intermediate structure mimicking the transition state of the initiation step. **b**, A schematic representation of the transition state of the elongation step. The side chain of Lys48 on Ub-Degron attacks the thioester bond of Ubc2-Ub. The inset shows

the designed intermediate structure mimicking the transition state of the elongation step. **c**, A brief synthetic route of the intermediate structure mimicking the transition state of the elongation step. **d**, A gel filtration chromatogram of Ubr1 (left) and an SDS-PAGE gel of purified Ubr1 and designed stable intermediate structures Ubc2-Ub-Degron and Ubc2-Ub-Ub-Degron (right).



Extended Data Fig. 4 | Cryo-EM density of the initiation and elongation complexes. **a**, Individual domains of Ubr1 in the initiation complex. **b**, Ubc2 and Ub in the initiation complex. **c**, Ubc2, donor Ub and acceptor Ub in the elongation complex. Maps in **a** and **b** were sharpened using a *B* factor of -96.5 \AA^2 and contoured at a level of 0.030. Maps in **c** were sharpened using a *B* factor of -96.7 \AA^2 and contoured at a level of 0.022. **d**, Degron recognition site of the initiation complex. **e**, Active site of the initiation complex.

f, Three-domain junction of the initiation complex. **g**, Active site of the elongation complex. **h**, Acceptor Ub and Ubr1 binding interface in the elongation complex. **i**, Acceptor Ub and Ubc2 binding interface in the elongation complex. Dotted circles in **d** and **e** mark the unmodelled densities corresponding to the Degron peptide which are only visible at the lower contour levels. Atomic models could not be reliably built into the densities.

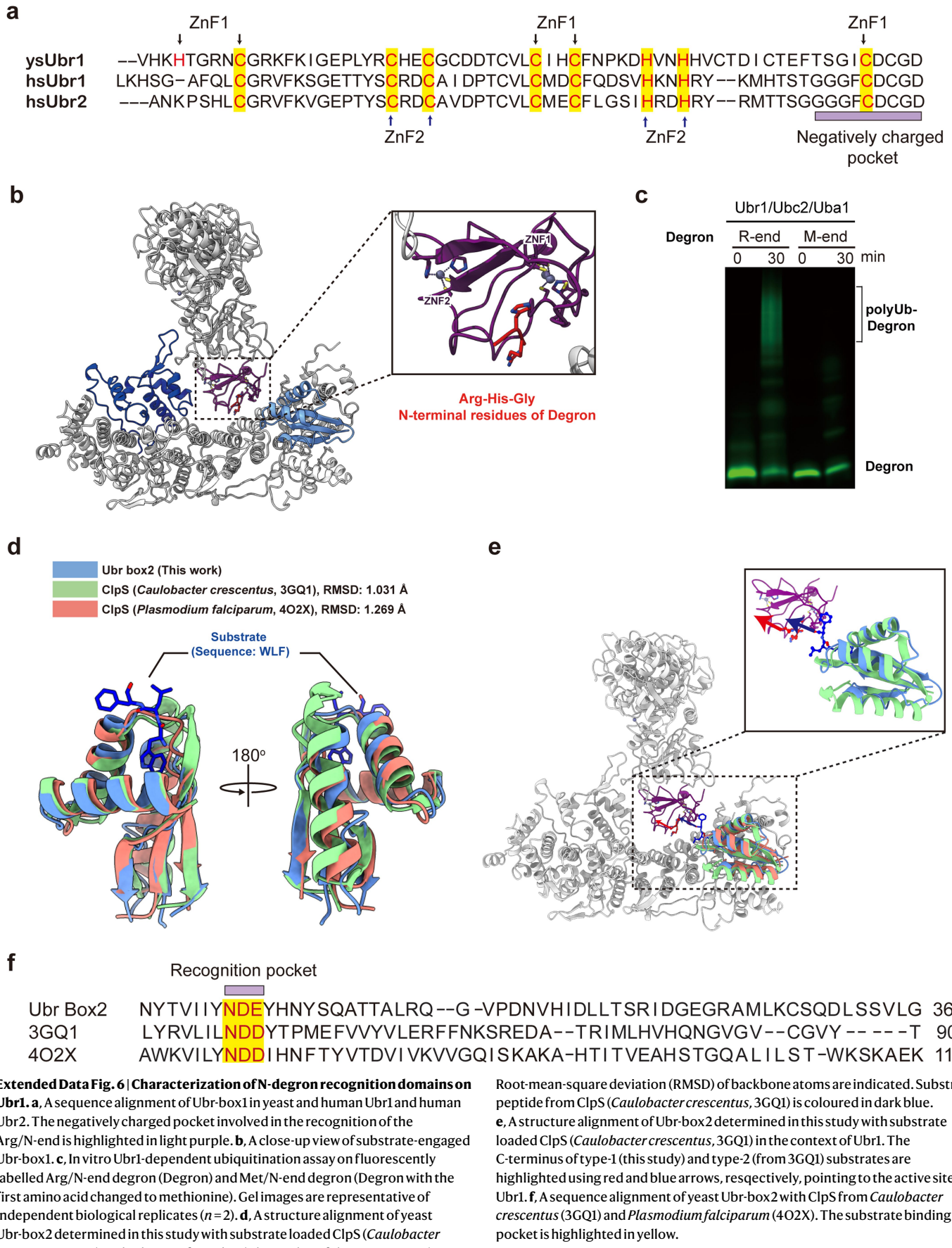


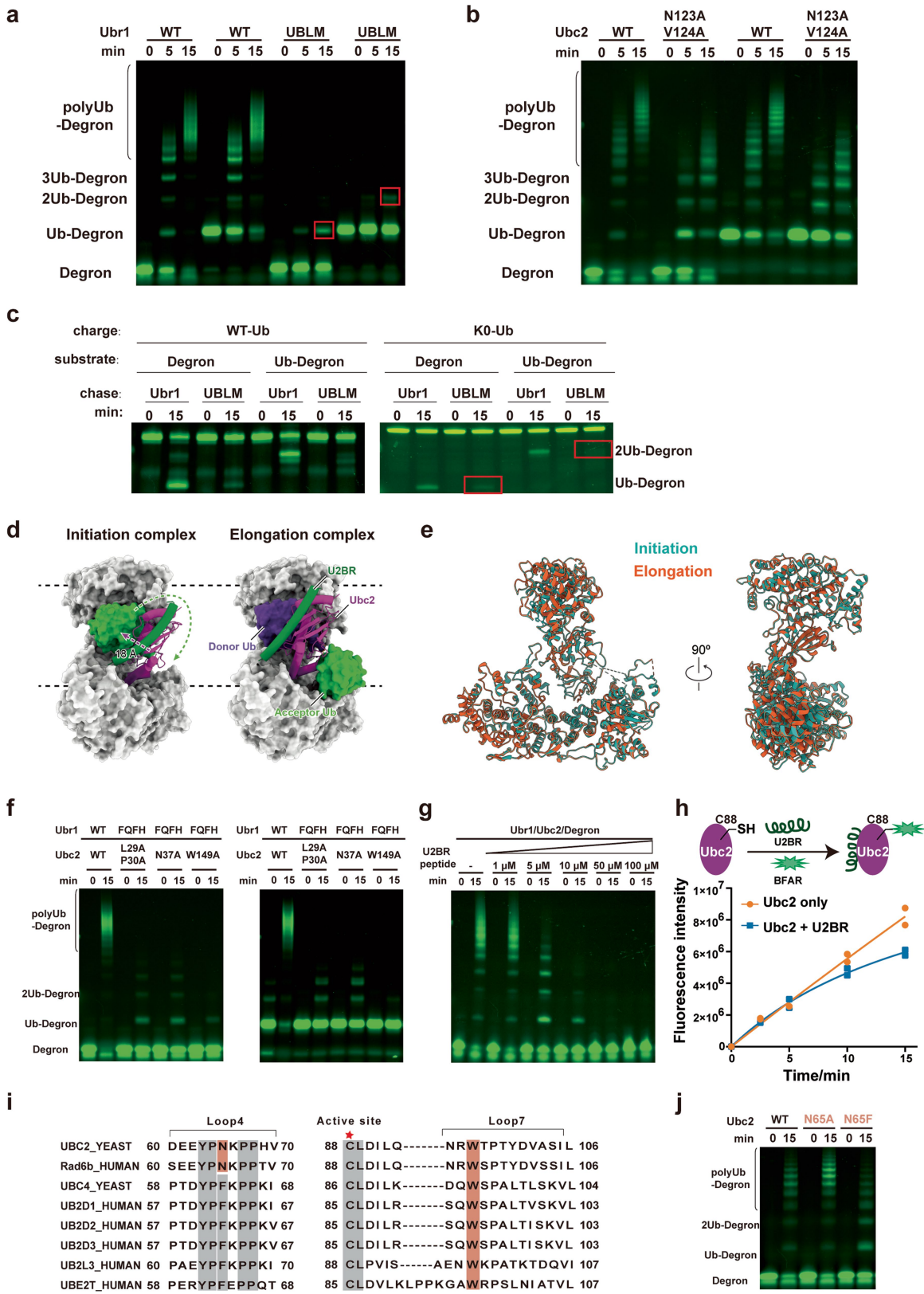
Extended Data Fig. 5 | See next page for caption.

Article

Extended Data Fig. 5 | Molecular structures of Ubr1 complex and interfaces between Ubr1 and Ub. **a**, The helical scaffold of Ubr1 consists of four separate regions. **b**, The three domains located around the helical scaffold, Ubr-Box1 (Ubox1, purple), Ubr-Box2 (Ubox2, light blue) and WHD (dark blue). **c**, The three domains above the helical scaffold, the RING finger domain (cyan), CHD (pink) and UBLC domain (yellow). The RING finger domain is sandwiched between the CHD and UBLC domain. An additional zinc finger motif (ZNF) in UBLC is labelled. **d**, U2BR (forest green), Ubc2 (magenta)–Ub (lime) and the RING finger domain form the catalytic module of Ubr1 complex. Two zinc finger motifs (ZNF) in the RING finger domain are labelled. **e**, Additional binding interfaces between the donor Ub and Ubr1 in the initiation complex, including K965 in

WHD, E1436 and Q1437 in CHD. R1783 in UBLC domain is the key residue to stabilize the loop of WHD. **f**, Additional binding interfaces between the acceptor Ub and Ubr1 in the elongation complex. **g**, *In vitro* Ubr1-dependent ubiquitination assay. A quadruple mutant (H161A, Y933A, D1175A, and H1763A, DHHY) of the residues involved in the interface between Ubox1, WHD, and UBLC (three-domain junction, shown in Fig. 1e) was tested. Gel images are representative of independent biological replicates ($n = 2$). **h**, *In vitro* Ubr1-dependent ubiquitination assay. Mutants of Ubr1 including K965A, E1436A/Q1437A, R1783A and K965A/E1436A/Q1437A/R1783A (KREQ) involved in the interfaces mentioned in **e** were tested. Gel images are representative of independent biological replicates ($n = 2$).

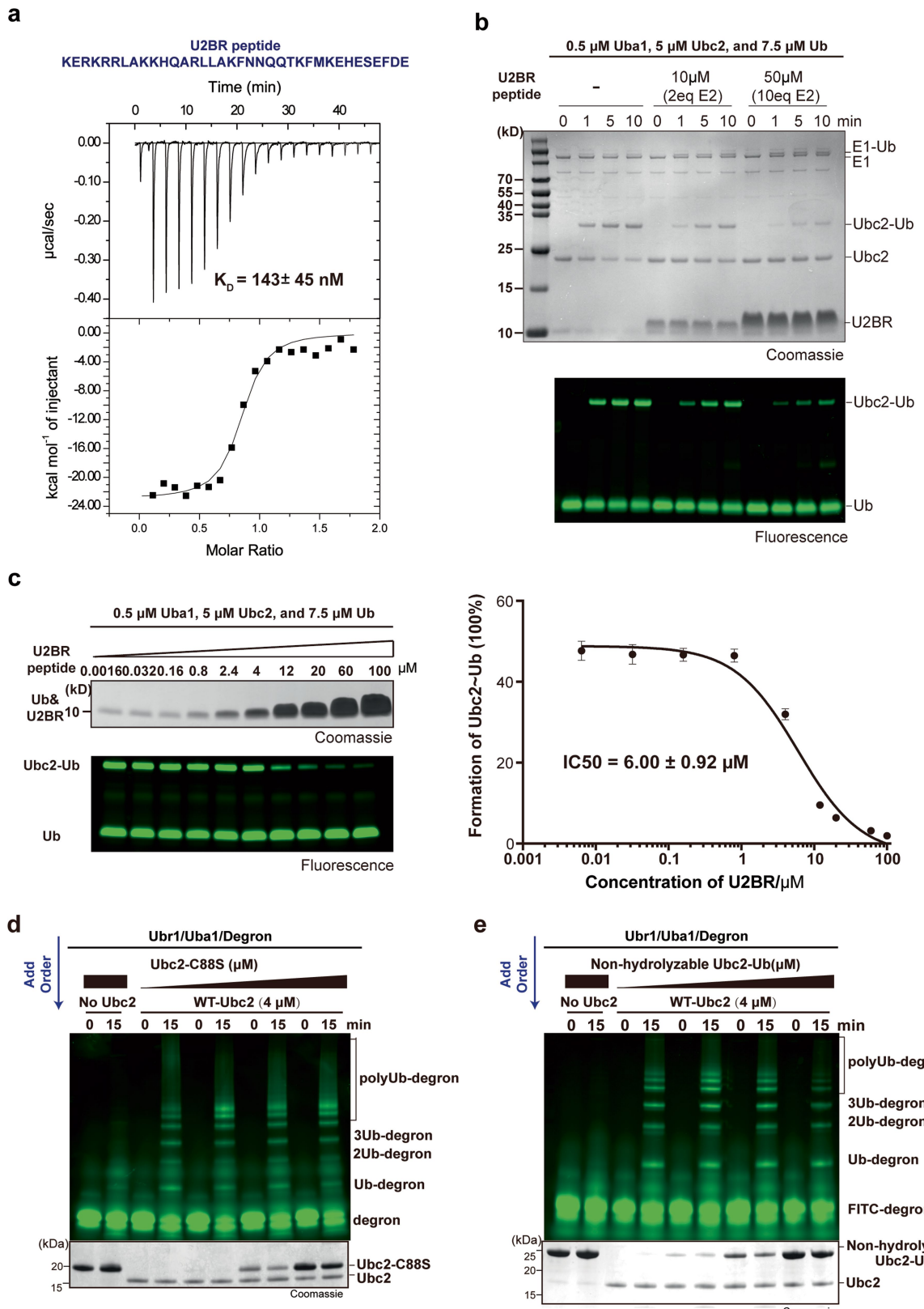




Extended Data Fig. 7 | See next page for caption.

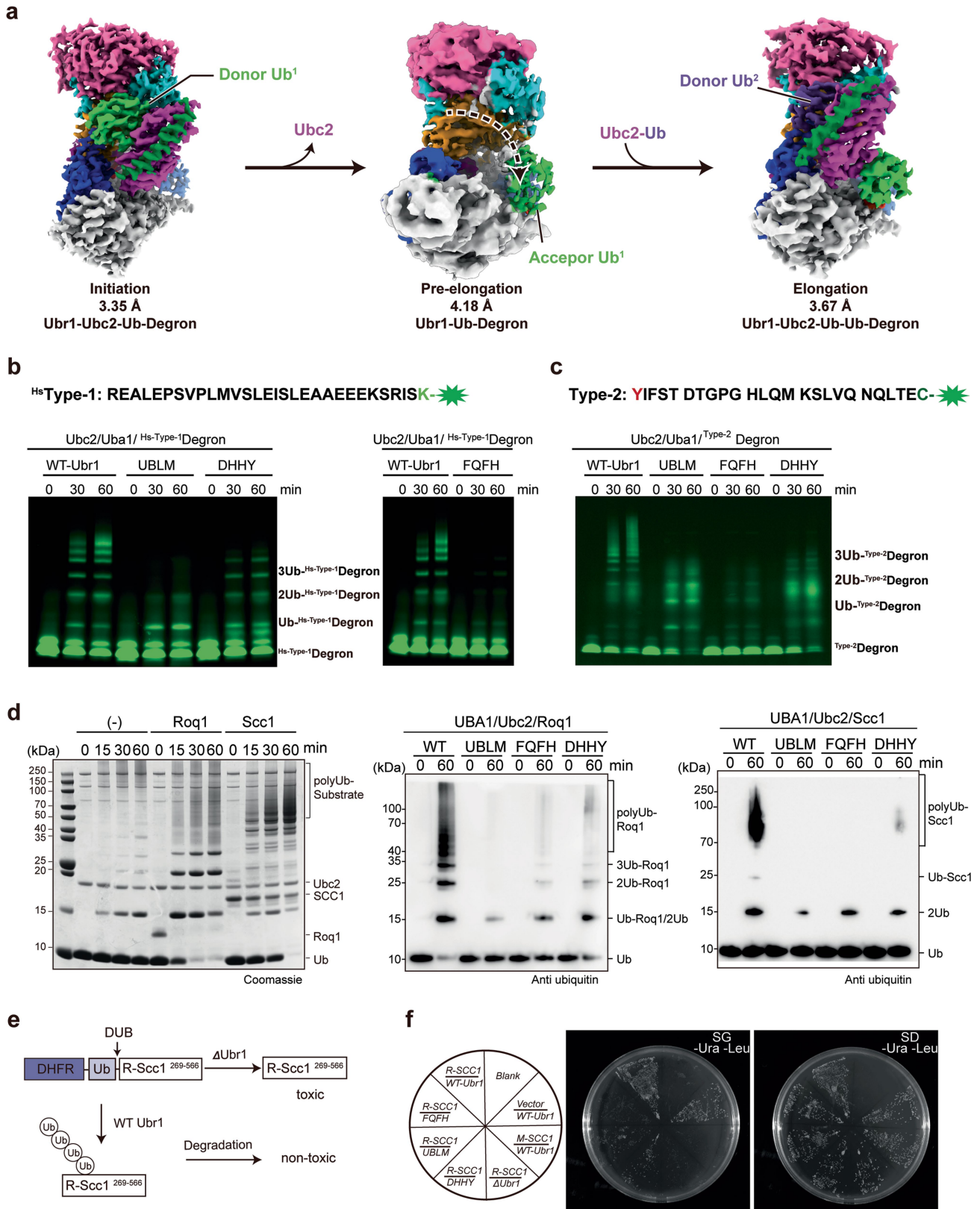
Extended Data Fig. 7 | Characterization of the interfaces between Ubr1, Ubc2 and Ub. **a–b.** In vitro Ubr1-dependent ubiquitination assays. Mutations of the Ub binding loop on Ubr1 (H678A/V679A/L680A/H681A, named UBLM mutant, **a**) and Ubc2 (N123A/V124A, **b**) were tested. Gel images are representative of independent biological replicates ($n=2$). Red boxes highlight the difference of UBLM mutant in initiation and elongation. **c.** Single-turnover ubiquitination assay of wild-type Ubr1 and UBLM mutant using Ubc2 charged with either wild-type Ub or Ub^{K0} (all Lysine residues mutated to Arginine). Red boxes highlight the defect of UBLM mutant in elongation. Gel images are representative of independent biological replicates ($n=2$). **d.** Side views of the initiation and elongation complexes showing the displacement of U2BR, Ubc2, and Ub. **e.** An alignment of Ubr1 structures in the initiation and elongation complexes. **f–g.** In vitro Ubr1-dependent ubiquitination assays. Gel images are representative

of independent biological replicates ($n=2$). **f.** Ubr1 (F1190A/Q1186A/F1183A/H1175A, named FQFH mutant) and Ubc2 mutants at the interface shown in Fig. 3b were tested. **g.** The inhibition of Ubr1-dependent ubiquitination in the presence of increasing concentrations of a synthetic U2BR peptide. **h.** The accessibility of the catalytic cysteine (Cys88) of Ubc2 was tested using fluorescein-5-maleimide, a bulky fluorescent alkylation reagent (BFAR), in the presence or absence of the synthetic U2BR peptide. The average fluorescence from two independent biological replicates was plotted ($n=2$). **i.** A sequence alignment of multiple E2 enzymes, including yeast and human Ubc2 (also known as Rad6b in human). Two regions involved in the interaction with the RING finger domain are shown. **j.** In vitro Ubr1-dependent ubiquitination assays were performed to examine the role of Asn65 of Ubc2 in the interaction with the RING finger domain of Ubr1. Gel images are representative of independent biological replicates ($n=2$).



Extended Data Fig. 8 | Characterization of the interactions between U2BR and Ubc2. **a**, ITC measurement of the binding between Ubc2 and the synthetic U2BR peptide. **b**, The formation of E1-dependent Ubc2-Ub thioester in the presence of the synthetic U2BR peptide. Gel images are representative of independent biological replicates ($n = 2$). **c**, Quantitative evaluations of the inhibitory effect of the synthetic U2BR peptide on E1-dependent Ubc2-Ub thioester formation. Averages of three independent biological replicates

($n = 3$) were plotted and fit to estimate the IC50 of the synthetic U2BR peptide. The curves are presented as mean values \pm s.d. **d–e**, In vitro Ubr1-dependent ubiquitination assay. Increasing doses of catalytically inactive Ubc2-C88S (**d**) and non-hydrolyzable Ubc2-Ub (**e**) up to 12.5 μM were pre-mixed with Ubr1, followed by adding wild-type Ubc2 at 4 μM . Gel images are representative of independent biological replicates ($n = 2$).



Extended Data Fig. 9 | See next page for caption.

Article

Extended Data Fig. 9 | The structure of the pre-elongation complex and validation of the structural mechanism. **a**, A comparison of initiation, pre-elongation and elongation complex in the same orientation showing the movement of ubiquitin. The colour code of Ubr1 is the same as that in Fig. 1b. Sharpened map of the pre-elongation complex is shown at a contour level of 0.011. **b**, In vitro ubiquitination assay on fluorescently labelled ¹¹⁸S-type-1 Degron (derived from human protein Rec8) with wild-type Ubr1 and Ubr1 mutants, UBLM, DHHY and FQFH. Gel images are representative of independent biological replicates ($n=2$). **c**, In vitro ubiquitination assay on fluorescently labelled Type-2 Degron (derived from Sindbis virus polymerase nsP4) with wild-type Ubr1 and Ubr1 mutants, UBLM, DHHY and FQFH. Gel images are representative of independent biological replicates ($n=2$). **d**, In vitro ubiquitination assay on truncated protein substrates ROQ1 (22-104) and Scc1 (268-384) with wild-type Ubr1 and Ubr1 mutants, UBLM, DHHY and FQFH. Gel

images are representative of independent biological replicates ($n=2$). **e**, The design of the yeast-growth assay. Endogenous deubiquitinating enzymes (DUB) cleave the construct co-translationally and produce Scc1 fragment (R-Scc1²⁶⁹⁻⁵⁶⁶) which has an N-terminal arginine residue and is toxic to the yeast strain deficient of Ubr1 ($\Delta UBR1$). If wild-type Ubr1 is supplemented, R-Scc1²⁶⁹⁻⁵⁶⁶ will be rapidly polyubiquitinated and degraded, reversing the growth defect. **f**, Yeast strains carrying wild-type Ubr1 or Ubr1 mutants (FQFH, UBLM and DHHY) were streaked either on dextrose-containing (SD) plates (right) where all strains grew without the expression of Scc1 fragment and Ubr1 variants, or on galactose containing (SG) plates (left), where all strains grew with the induced gene expression of Scc1 fragment and Ubr1 variants. In addition to R-Scc1²⁶⁹⁻⁵⁶⁶, M-Scc1²⁶⁹⁻⁵⁶⁶ which has an N-terminal methionine residue was also tested. The plates were incubated at 30 °C for 3 d.

Extended Data Table 1 | Cryo-EM data collection, refinement and validation statistics

	Initiation complex (EMDB-23806) (PDB 7MEX)	Elongation complex (EMDB-23807) (PDB 7MEY)	Pre-elongation complex (EMDB-24935)	Apo-Ubr1 (EMDB-24936)
Data collection and processing				
Magnification	81,000	81,000	81,000	81,000
Voltage (kV)	300	300	300	300
Electron exposure (e ⁻ /Å ²)	50	50	50	50
Defocus range (μm)	-1.0 to -2.5	-1.0 to -2.5	-1.0 to -2.5	-1.0 to -2.5
Pixel size (Å)	1.063	1.063	1.065	1.122
Symmetry imposed	C1	C1	C1	C1
Initial particle images (no.)	1,643,874	646,482	1,765,032	636,808
Final particle images (no.)	232,915	65,088	193,669	30,415
Map resolution (Å)	3.35	3.67	4.18	4.56
FSC threshold	0.143	0.143	0.143	0.143
Refinement				
Model resolution (Å)	3.46	3.83		
FSC threshold	0.5	0.5		
Map sharpening <i>B</i> factor (Å ²)	-96.5	-96.7		
Model composition				
Non-hydrogen atoms	15941	16468		
Protein residues	1967	2033		
Ligands	Zn: 7	Zn: 7		
		ETE: 1 (chemical linker)		
<i>B</i> factors (Å ²)				
Protein	43.78	87.17		
Ligand	70.81	122.04		
R.m.s. deviations				
Bond lengths (Å)	0.003	0.003		
Bond angles (°)	0.519	0.541		
Validation				
MolProbity score	1.48	1.75		
Clashscore	8.11	10.74		
Poor rotamers (%)	0.06	0.00		
Ramachandran plot				
Favored (%)	97.84	96.77		
Allowed (%)	2.16	3.23		
Disallowed (%)	0.00	0.00		

Reporting Summary

Nature Research wishes to improve the reproducibility of the work that we publish. This form provides structure for consistency and transparency in reporting. For further information on Nature Research policies, see our [Editorial Policies](#) and the [Editorial Policy Checklist](#).

Statistics

For all statistical analyses, confirm that the following items are present in the figure legend, table legend, main text, or Methods section.

n/a Confirmed

The exact sample size (n) for each experimental group/condition, given as a discrete number and unit of measurement

A statement on whether measurements were taken from distinct samples or whether the same sample was measured repeatedly

The statistical test(s) used AND whether they are one- or two-sided
Only common tests should be described solely by name; describe more complex techniques in the Methods section.

A description of all covariates tested

A description of any assumptions or corrections, such as tests of normality and adjustment for multiple comparisons

A full description of the statistical parameters including central tendency (e.g. means) or other basic estimates (e.g. regression coefficient) AND variation (e.g. standard deviation) or associated estimates of uncertainty (e.g. confidence intervals)

For null hypothesis testing, the test statistic (e.g. F , t , r) with confidence intervals, effect sizes, degrees of freedom and P value noted
Give P values as exact values whenever suitable.

For Bayesian analysis, information on the choice of priors and Markov chain Monte Carlo settings

For hierarchical and complex designs, identification of the appropriate level for tests and full reporting of outcomes

Estimates of effect sizes (e.g. Cohen's d , Pearson's r), indicating how they were calculated

Our web collection on [statistics for biologists](#) contains articles on many of the points above.

Software and code

Policy information about [availability of computer code](#)

Data collection	Cryo-EM: ThermoFisher EPU installed on Titan Krios microscope at the Advanced Electron Microscopy Facility at the University of Chicago, Gatan Latitude S installed on Titan Krios microscope at the National Cryo-EM Facility.
Data analysis	GraphPad Prism v8.2.1; Cryo-EM: MotionCor2 v1.3.2, CTFFIND v4.1.9, RELION v3.1; Structure Visualization: ChimeraX v0.9; Model Building: COOT v0.89, PHENIX v1.15.2.

For manuscripts utilizing custom algorithms or software that are central to the research but not yet described in published literature, software must be made available to editors and reviewers. We strongly encourage code deposition in a community repository (e.g. GitHub). See the Nature Research [guidelines for submitting code & software](#) for further information.

Data

Policy information about [availability of data](#)

All manuscripts must include a [data availability statement](#). This statement should provide the following information, where applicable:

- Accession codes, unique identifiers, or web links for publicly available datasets
- A list of figures that have associated raw data
- A description of any restrictions on data availability

Cryo-EM maps have been deposited in the Electron Microscopy Data Bank (EMDB, www.ebi.ac.uk/pdbe/emdb/) under the accession codes EMDB-23806 (initiation complex), EMDB-23807 (elongation complex), EMDB-24935 (pre-elongation complex), and EMDB-24936 (apo-Ubr1). The atomic models have been deposited in the Protein Data Bank (PDB, www.rcsb.org) under the accession codes 7MEX (initiation complex) and 7MEY (elongation complex). The atomic model of UbcH5 and the RING finger domain of TRIM25 is available under the PDB accession code 5FER. Uncropped gels and blots source data have been included as Supplementary Information Fig. 7. Due to the large file size, raw electron microscopy data are available from the corresponding authors upon request.

Field-specific reporting

Please select the one below that is the best fit for your research. If you are not sure, read the appropriate sections before making your selection.

Life sciences Behavioural & social sciences Ecological, evolutionary & environmental sciences

For a reference copy of the document with all sections, see nature.com/documents/nr-reporting-summary-flat.pdf

Life sciences study design

All studies must disclose on these points even when the disclosure is negative.

Sample size	The work performed here did not involve statistical analyses that would be impacted by sample size.
Data exclusions	No data was excluded.
Replication	The ubiquitination assays were performed with two independent biological replicates. All attempts at replication were successful.
Randomization	Randomization is not relevant for the structural analysis described in this study, because no grouped samples were involved.
Blinding	Blinding is not relevant for the structural analysis described in this study, because no grouped samples were involved.

Reporting for specific materials, systems and methods

We require information from authors about some types of materials, experimental systems and methods used in many studies. Here, indicate whether each material, system or method listed is relevant to your study. If you are not sure if a list item applies to your research, read the appropriate section before selecting a response.

Materials & experimental systems		Methods	
n/a	Involved in the study	n/a	Involved in the study
<input checked="" type="checkbox"/>	<input type="checkbox"/> Antibodies	<input checked="" type="checkbox"/>	<input type="checkbox"/> ChIP-seq
<input checked="" type="checkbox"/>	<input type="checkbox"/> Eukaryotic cell lines	<input checked="" type="checkbox"/>	<input type="checkbox"/> Flow cytometry
<input checked="" type="checkbox"/>	<input type="checkbox"/> Palaeontology and archaeology	<input checked="" type="checkbox"/>	<input type="checkbox"/> MRI-based neuroimaging
<input checked="" type="checkbox"/>	<input type="checkbox"/> Animals and other organisms		
<input checked="" type="checkbox"/>	<input type="checkbox"/> Human research participants		
<input checked="" type="checkbox"/>	<input type="checkbox"/> Clinical data		
<input checked="" type="checkbox"/>	<input type="checkbox"/> Dual use research of concern		